

Heavy-quark initiated charged-current deep-inelastic scattering coefficient functions through $\mathcal{O}(\alpha_s^2)$

Kirill Kudashkin

School of Physics, Shandong University, Jinan, Shandong 250100, China

Tif Lab, Dipartimento di Fisica, Universit`a di Milano and INFN, Sezione di Milano, Via Celoria 16, I-20133 Milano, Italy

E-mail: kkudashkin@sdu.edu.cn

ABSTRACT: We compute the coefficient functions for heavy-quark initiated charged-current deep-inelastic scattering through $\mathcal{O}(\alpha_s^2)$, retaining full mass dependence for a single heavy-quark flavor. The calculation employs a cut-based approach to isolate individual diagram contributions and to derive differential equations for the relevant master integrals, which are solved analytically in terms of generalized polylogarithms. The results are presented in the decoupling scheme for n_L light active flavors, facilitating their direct implementation in variable-flavor number schemes such as ACOT and FONLL.

KEYWORDS: coefficient functions, deep-inelastic scattering, heavy flavor, intrinsic charm, NNLO, variable-flavor number scheme

Contents

1	Introduction	1
2	Theoretical setup for heavy-quark DIS	3
2.1	Formalism and conventions	3
2.2	Cut-based approach to scattering amplitudes	6
3	Computation of master integrals	9
3.1	Cut based approach to differential equations	9
3.2	Real-radiation: canonical transformations	12
3.3	Real-radiation: integration	13
3.4	Virtual: canonical transformations and integration	15
3.5	Boundary conditions	17
4	Results	18
4.1	Renormalization	18
4.2	Isolating soft contribution	20
4.3	Born coefficient functions	22
4.4	$\mathcal{O}(\alpha_s)$ coefficient functions	23
4.5	$\mathcal{O}(\alpha_s^2)$ coefficient functions	24
4.6	Auxiliary files and validation	28
5	Summary and outlook	30
Appendices		30
A	Auxiliaries	31
A.1	Parton kinematics	31
A.2	Projectors, normalization and γ_5 schemes	32
B	Master integrals material	33

1 Introduction

The role of heavy quarks, specifically the charm quark, in the proton structure has a long history in theoretical physics. It began with the work of Witten [1], who established that charm quarks and antiquarks inside the proton are generated primarily via the dynamical mechanism of perturbative Quantum Chromodynamics (pQCD), known as *extrinsic* production. Shortly thereafter, Brodsky et al. [2] proposed that the proton wave function could contain a non-perturbative *intrinsic* charm component arising from quantum fluctuations.

Deep-inelastic scattering (DIS) at high-energy colliders offers the essential experimental framework to resolve and study both contributions [3].

At present, parton distribution functions (PDFs), describing the dynamics of quarks and gluons inside hadrons, are extracted through a global QCD fit that combines data spanning a wide energy range from various experiments (CTEQ [4, 5], MSHT [6, 7], NNPDF [8, 9], and PDF4LHC [10]). A dedicated theoretical framework is required to incorporate heavy-quark mass effects consistently across this wide energy range. Building on the foundation laid by [1, 2], variable-flavor number schemes (VFNS) such as ACOT [11, 12] (and its modifications from e.g. [13, 14]) and FONLL [15–17], provide such framework by implementing perturbative matching conditions between pQCD calculations with different numbers of active quark flavors.

The purpose of a VFNS is to interpolate between two characteristic kinematic regimes: the high-energy regime $Q^2/m_Q^2 \gg 1$ (Q^2 being the typical pQCD scale, m_Q^2 the heavy-quark mass squared), where large logarithms of this ratio dominate, and the threshold region $Q^2 \approx m_Q^2$, where finite-mass effects are essential [11, 12, 16]. The interpolation is realized through universal PDF matching conditions that are most directly obtainable through two complementary approaches: via the operator product expansion [18], or by explicit calculation using DIS coefficient functions as the suitable observable [19]. Accordingly, the accuracy of a global QCD fit in a VFNS relies on the availability of high-order pQCD calculations. The charged-current DIS coefficient functions computed here provide precisely this necessary input, from which, in principle, the matching conditions can be subsequently extracted and the VFNS implemented.

Such calculations have now reached $\mathcal{O}(\alpha_s^3)$ accuracy, corresponding to third-order (N³LO) corrections to the leading QCD contribution for the dominant extrinsic production channel in DIS-related observables [20–27]. In contrast, pQCD calculations relevant for constraining the intrinsic charm component of PDFs have seen comparatively little advancement over the past two decades — the state of the art for this channel remains $\mathcal{O}(\alpha_s)$ (NLO) [28–30]. The primary reason for this is the small integrated momentum fraction carried by intrinsic charm, estimated to be only about 1–2% of the total proton momentum [2, 31]. Consequently, global QCD fits, more often than not, adopt the simplifying ansatz of a radiatively generated charm sea, explicitly excluding any intrinsic contribution.

“However, nature does not have to subscribe to this scenario” [31]. A recent NNPDF global analysis revisited the intrinsic charm hypothesis [32], presenting evidence for its existence. To move from evidence to a definitive conclusion, improvements in experimental and theoretical directions are mandatory.

Several experimental programs directly probe the proton’s charm content or provide complementary constraints. At the LHC, dedicated forward neutrino experiments like FASER ν [33] and SND@LHC [34] will provide up to one million new DIS events by the end of the HL-LHC. They will cover a larger kinematic range than previous experiments and are projected to significantly constrain PDF uncertainties [35]. Furthermore, a potentially powerful probe of intrinsic charms arises from the study of atmospheric neutrino fluxes. It has been shown recently [36] that while including an intrinsic charm component does not fully reconcile existing discrepancies between IceCube measurements [37] and theoretical

predictions for the muon neutrino flux, it identifies the high-energy atmospheric neutrino spectrum as a sensitive and largely unexplored observable for this kind of physics. For other experimental avenues, we refer to the dedicated study [14], which estimates the sensitivity of different DIS experiments to heavy-quark mass effects.

To benefit from the forthcoming data, the high-energy community is actively advancing toward N^3LO global QCD fits [5, 38, 39]. In light of this goal, the stark imbalance between pQCD calculations for intrinsic charm (currently $\mathcal{O}(\alpha_s)$) and extrinsic charm (now at $\mathcal{O}(\alpha_s^3)$) represents a critical bottleneck. Without $\mathcal{O}(\alpha_s^2)$ correction for the intrinsic channel, its associated theoretical uncertainty remains uncontrolled at the precision targeted by N^3LO fits, potentially biasing the extraction or exclusion of an intrinsic charm component. We address this issue directly by providing the first calculation of the $\mathcal{O}(\alpha_s^2)$ corrections for heavy-quark initiated charged-current DIS, thereby providing essential NNLO corrections for a consistent theoretical treatment of the intrinsic charm component.

The paper is organized as follows. Sec. 2 lays out the theoretical framework for heavy quark DIS, defining our notation and detailing the cut-based approach used to isolate the relevant contributions to the coefficient functions. The core computational machinery is presented in Sec. 3, which describes the derivation of differential equations for the master integrals, their transformation to canonical form, and their subsequent integration for both real-radiation and virtual contributions. At the end of this section, we cover the determination of integration constants via the PSLQ algorithm. Sec. 4 presents the renormalized coefficient functions, discussing the renormalization scheme, the regularization of soft singularities, and providing explicit expressions for the Born, $\mathcal{O}(\alpha_s)$, and $\mathcal{O}(\alpha_s^2)$ coefficient functions, along with details on the auxiliary files and validation. A summary and outlook are given in Sec. 5. Technical details on kinematics, projectors, and γ_5 schemes are collected in App. A, while materials related to the master integrals are provided in App. B.

2 Theoretical setup for heavy-quark DIS

In this section, we provide the technical details for the computation of corrections to the partonic DIS structure functions up to and including $\mathcal{O}(\alpha_s^2)$. First, we present the formulae relevant to all specified perturbative orders, including the normalization of the coefficient functions, tensor decomposition, and etc. We then introduce the computational techniques, with a particular focus on the application of cut-based methods to the computation of scattering amplitudes.

2.1 Formalism and conventions

We consider deep-inelastic scattering mediated by a charged-current, specifically by the exchange of a virtual $W^-(q)$ boson with a nucleon P ,

$$W^-(q) + P(P) \rightarrow X, \quad (2.1)$$

where X denotes the inclusive hadronic final state. In the following, we focus solely on the hadronic tensor, leaving the leptonic part out of the discussion. We refer to [11] for further details.

The hadronic tensor for the process in Eq. (2.1) is defined in the standard manner as

$$W^{\mu\nu} = \frac{1}{4\pi} \sum_{\mathbf{X}} \sum_{\text{spin}} \langle \mathbf{P} | J^\mu | \mathbf{X} \rangle \langle \mathbf{X} | (J^\nu)^\dagger | \mathbf{P} \rangle (2\pi)^4 \delta^{(4)}(P + q - p_{\mathbf{X}}), \quad (2.2)$$

where J^μ is the charged weak current and the sum runs over all hadronic final states \mathbf{X} with momentum $p_{\mathbf{X}}$.

In the Bjorken limit, the dominant contribution to the hadronic tensor assumes a factorized form [11, 12],

$$W^{\mu\nu}(x_B, Q^2, m^2) = \sum_n \int_\eta^1 \frac{d\xi}{\xi} f_n(\xi, \mu^2) \widehat{\omega}_n^{\mu\nu} \left(\frac{\eta}{\xi}, \mu^2, Q^2, m^2 \right) + \mathcal{O} \left(\frac{\Lambda}{Q} \right), \quad (2.3)$$

where the sum runs over all parton species. Λ denotes a generic nonperturbative QCD scale, $\eta = \eta(x_B)$ is the generalized Bjorken variable defined in Eq. (A.3), and $f_n(\xi, \mu^2)$ is the parton distribution function for parton n carrying a light-cone momentum fraction $\xi \equiv p^+/P^+$ at factorization scale μ .

We work in the massive ACOT factorization scheme, which consistently retains heavy-quark mass effects and whose validity is established within the framework of the QCD factorization theorem [40]. In this framework, the factorized hadronic tensor involves finite, mass-factorized partonic tensors $\widehat{\omega}_n^{\mu\nu}$. In the present work, however, we compute the corresponding massive, ultraviolet-renormalized but *ACOT-unsubtracted* partonic tensor $\omega_n^{\mu\nu}$ through $\mathcal{O}(\alpha_s^2)$ for heavy-quark initiated charged-current deep-inelastic scattering. The matching to the massless $\overline{\text{MS}}$ scheme and the resummation of quasi-collinear large logarithms are deferred to a future publication [41].

The partonic tensor, which describes the hard scattering of the virtual boson off an incoming parton n , is defined as

$$\omega_n^{\mu\nu} = \sum_{\mathbf{X}_{\text{QCD}}} \overline{\sum_{\text{color, spin}}} \langle n | J^\mu | \mathbf{X}_{\text{QCD}} \rangle \langle \mathbf{X}_{\text{QCD}} | (J^\nu)^\dagger | n \rangle, \quad (2.4)$$

where the bar indicates averaging over the initial parton's color and spin, and the sum runs over all QCD final states \mathbf{X}_{QCD} at the given perturbative order.

Its perturbative expansion in $\alpha_s = g_s^2/(4\pi)$ reads

$$\omega_n^{\mu\nu} = \sum_{k=0}^{\infty} \left(\frac{\alpha_s}{2\pi} \right)^k \omega_n^{(k),\mu\nu}, \quad (2.5)$$

where $\omega_n^{(k),\mu\nu}$ comprises all contributions of order α_s^k . All quantities in this section are understood to be renormalized; details of the renormalization scheme choice are given in Sec. 4.1.

Specifically, we consider the process where the incoming parton is a heavy quark Q (or antiquark \bar{Q}), identified as charm ($Q \equiv c$), and the outgoing quark is massless¹

$$W^-(q) + Q(p)/\bar{Q}(p) \rightarrow q/\bar{q} + \mathbf{X}_{\text{QCD}}. \quad (2.6)$$

¹We focus on W^- initiated processes; the charge-conjugated W^+ channels follow by symmetry, and all formulas below are given for the W^- case.

We adopt $n_F = 4$ quark flavors, with $n_L = 3$ light flavors (u, d, s) and $n_H = 1$ heavy flavor. The relevant Mandelstam invariants are

$$q^2 = -Q^2 < 0, \quad p^2 = m^2 > 0, \quad s = (q+p)^2. \quad (2.7)$$

The charged weak current operator is given by:

$$J^\mu = \bar{q}_\alpha \gamma^\mu (V - A \gamma_5) \mathcal{V}_{\alpha\beta} q_\beta, \quad (2.8)$$

where V and A are the vector and axial-vector couplings, kept general for now; their standard values are $V = A = -ig/\sqrt{2}$, with g the weak coupling constant. The Cabibbo-Kobayashi-Maskawa (CKM) matrix $\mathcal{V}_{\alpha\beta}$ for $n_F = 4$ is

$$\mathcal{V}_{\alpha\beta} = \begin{bmatrix} V_{ud} & V_{us} \\ V_{cd} & V_{cs} \end{bmatrix}, \quad (2.9)$$

which induces the flavor decomposition of the partonic tensor

$$\omega_n^{\mu\nu} \equiv |V_{ud}|^2 \omega_{n,ud}^{\mu\nu} + |V_{us}|^2 \omega_{n,us}^{\mu\nu} + |V_{cd}|^2 \omega_{n,cd}^{\mu\nu} + |V_{cs}|^2 \omega_{n,cs}^{\mu\nu}. \quad (2.10)$$

Because the DIS process we consider is initiated exclusively by a heavy quark (or antiquark) and we work through $\mathcal{O}(\alpha_s^2)$, the set of *unique* Feynman diagrams contributing to the coefficient functions (Tab. 1) is obtained from the channels $\omega_{n,cs}^{\mu\nu}$ and $\omega_{n,ud}^{\mu\nu}$ alone (cf. Fig. 1). To avoid proliferation of indices, we suppress the explicit flavor labels in the following and work with these flavor-stripped tensors. We will restore the appropriate CKM factors explicitly whenever a distinction between the individual flavor channels is required.

	$\mathcal{O}(\alpha_s^0)$	$\mathcal{O}(\alpha_s^1)$	$\mathcal{O}(\alpha_s^2)$					
	B	V	R	VV	RV	RRA	RRB	RRC
X _{QCD}	q	q	gq	q	gq	ggq, $\tilde{g}\tilde{g}q$, $\bar{q}qq$	$\bar{Q}Qq$	$Q\bar{q}q$
N	1		5			106		

Table 1: Intermediate states contributing to the coefficient functions at different orders in perturbation theory. Abbreviations: B (Born contribution), V (virtual contribution), R (real contribution), VV (double virtual contribution), RV (real-virtual contribution), RRA, RRB and RRC (different real-real contributions). The bottom row lists the number N of the corresponding unique forward scattering amplitudes contributing to the coefficient functions.

Following the normalization of Ref. [28], the amplitude is decomposed into tensors as follows:

$$\omega^{\mu\nu} = -\omega_1 \eta^{\mu\nu} + \omega_2 p_2^\mu p_2^\nu + i\omega_3 \varepsilon^{\mu\nu\alpha\beta} p_{1,\beta} p_{2,\alpha} + \omega_4 p_1^\mu p_1^\nu + \omega_5 (p_1^\mu p_2^\nu + p_2^\mu p_1^\nu), \quad (2.11)$$

where $\eta^{\mu\nu}$ is the Minkowski metric and ε is the Levi-Civita symbol. Our goal is to compute the NNLO QCD correction to the dominant structure functions. We omit the contributions of ω_4 and ω_5 , as they are suppressed by powers of the lepton mass from the lepton vertex.²

²We note, however, that a recent NLO analysis suggests the corresponding structure functions can be relevant in certain cases [29, 30]. There is no conceptual difficulty in computing ω_4 and ω_5 within our framework, but such a calculation lies beyond the original goal of the present publication.

The form factors in Eq. 2.11 are projected out as follows:

$$\omega_i = \mathcal{P}_i^{\mu\nu} \omega_{\mu\nu}. \quad (2.12)$$

Due to known technical issues with γ_5 in higher-order calculations, we employ two different schemes that address them: the mutual agreement of results obtained in these two schemes ensures the correctness of the underlying calculations. The projectors \mathcal{P}_i are therefore derived in accordance with the γ_5 schemes discussed in App. A.2.

Upon applying the projectors defined above to Eq. (2.3) we obtain the (scaling) hadronic structure functions

$$\begin{aligned} F_1 &= \sum_{n=Q,\bar{Q}} \int_{\eta}^1 \frac{d\xi}{\xi} f_n(\xi, \mu^2) C_{1,n}, \\ F_2 &= \sum_{n=Q,\bar{Q}} \int_{\eta}^1 \frac{d\xi}{\xi} f_n(\xi, \mu^2) C_{2,n}, \\ F_3 &= \sum_{n=Q,\bar{Q}} \int_{\eta}^1 \frac{d\xi}{\xi} f_n(\xi, \mu^2) C_{3,n}, \end{aligned} \quad (2.13)$$

where

$$C_{j,n} = \mathcal{N}_j \omega_{j,n} \quad (j = 1, 2, 3), \quad (2.14)$$

with the normalization factors [11, 28]

$$\begin{aligned} \mathcal{N}_1 &= \frac{1}{4\pi}, \\ \mathcal{N}_2 &= \frac{2x_B}{8\pi} \frac{\Delta^2[-Q^2, m^2, s]}{2Q^2}, \\ \mathcal{N}_3 &= \frac{1}{4\pi} \Delta[-Q^2, m^2, s]. \end{aligned} \quad (2.15)$$

Here, x_B is the Bjorken-scaling variable and Δ is the triangle function (see App. A.1 for definitions).

2.2 Cut-based approach to scattering amplitudes

The coefficient functions follow from the optical theorem, which relates the hadronic tensor $\omega^{\mu\nu}$ to the forward Compton amplitude [42]

$$\omega^{\mu\nu} = 2 \operatorname{Im} \mathcal{M}^{\mu\nu}. \quad (2.16)$$

This identity allows us to compute the structure functions either by calculating $\mathcal{M}^{\mu\nu}$ directly or by extracting the individual contributions listed in Tab. 1 from its imaginary part via cut techniques.³

To achieve the latter, we identify the cuts of each Feynman diagram contributing to the forward scattering amplitude \mathcal{M} using the approach of Refs. [43–45]. In those works,

³For the remainder of the paper, we do not distinguish between the structure functions and the forward scattering amplitude and use both interchangeably unless stated otherwise.

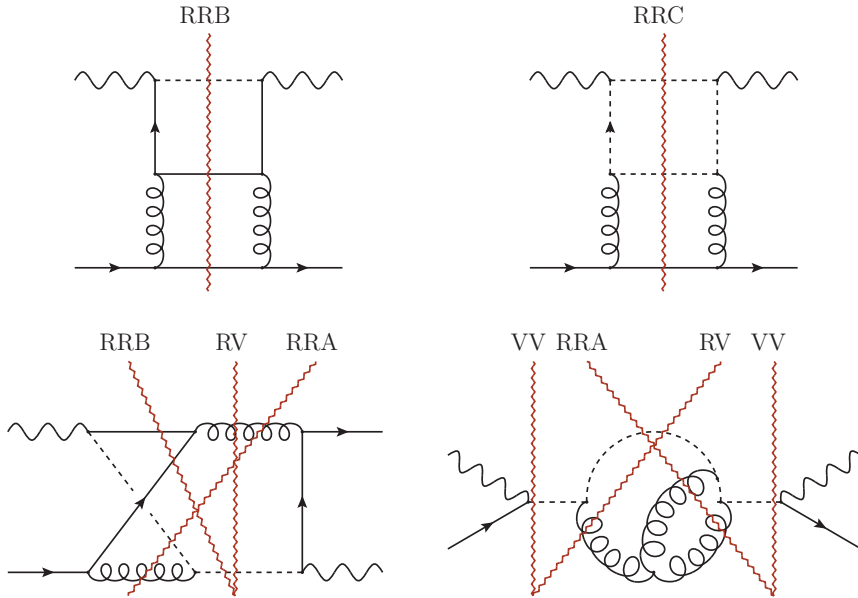


Figure 1: Typical Compton diagrams that appear in the calculations. Here, a solid line indicates a heavy quark propagator, a dashed line indicates a light quark propagator, a wavy line indicates the external boson, and a curly line represents a gluon propagator. Zigzag lines represent the cuts (cf. Tab. 3). The right diagram in the top row, and similar sea diagrams, appear in the coefficient functions proportional to $\omega_{n,ud}^{\mu\nu}$, while other diagrams are typical for $\omega_{n,cs}^{\mu\nu}$.

the problem of finding all possible cuts of the given graph (Feynman diagram) is mapped onto the graph-theoretic problem of graph coloring. Computational algorithms for this task rely on the adjacency matrix of a Feynman diagram, which is straightforwardly obtained from the output of graph generators like **QGRAF** [46]. Public implementations are available, e.g., in the **Mathematica** package **TOPOID** [47] and in **FeynCalc** [48, 49].⁴ For this work, we employ our own implementation of the algorithms described in Refs. [43, 45].

We generate all graphs for the bare forward two-loop Compton amplitude using **QGRAF** and extract their adjacency matrices (typical two-loop diagrams are shown in Fig. 1). The initial set contains graphs that possess no physical s -channel cuts (i.e., they do not contribute to the imaginary part of the forward-scattering amplitude). Directly filtering these graphs is cumbersome without ad-hoc modifications in **QGRAF**; instead, we apply the cut-identification algorithm described above to select only graphs with non-zero s -channel cuts, retaining 79 out of the original 112 graphs. The surviving graphs and their cut information are retained for subsequent extraction of the contributions listed in Tab. 1.

The filtered abstract graphs are then passed to **FORM** [50], where we apply Feynman rules (in Feynman gauge) to convert vertices and edges into explicit algebraic expressions. All subsequent algebraic manipulations are performed in **FORM** using a combination of standard packages, notably **color** [51] for $\mathfrak{su}(N)$ algebra, supplemented by private routines.

⁴We thank V. Shtabovenko for private communications on this matter.

These manipulations include color algebra, Dirac algebra, and operations with Lorentz tensors. Traces involving γ_5 are handled according to the schemes detailed in App. A.2. After applying the projectors, as defined in Eq. (A.11) and used in Eq. (2.12), the amplitude reduces to a linear combination of scalar Feynman integrals and rational functions of the kinematic variables and the space-time dimension d .

We work in dimensional regularization with $d = 4 - 2\epsilon$ to regulate both ultraviolet (UV) and infrared (IR) divergences that appear in the scattering amplitude. A generic scalar integral in this setting has the form

$$j = (\mu^2)^{2\epsilon} \int \frac{d^d l_1}{(2\pi)^d} \frac{d^d l_2}{(2\pi)^d} \frac{\mathcal{N}(l_1, l_2, p_1, p_2)}{D_1^{a_1} D_2^{a_2} D_3^{a_3} D_4^{a_4} D_5^{a_5} D_6^{a_6} D_7^{a_7}}, \quad (2.17)$$

where μ is the 't Hooft mass, introduced to keep the coupling dimensionless in d dimensions; if not mentioned otherwise, $\mu = Q \equiv 1$. Here, $D_i = L_i^2 - M_i^2 + i0$ are inverse propagators; L_i is a linear combination of the loop momenta l_1, l_2 and the external momenta p_1, p_2 , while M_i denotes the corresponding mass. The exponents a_i are integers, and $\mathcal{N}(l_1, l_2, p_1, p_2)$ is a polynomial in scalar products of the loop and external momenta.

Family	Propagators D_1, \dots, D_7
fam1	$(l_2 + p_1)^2 - m^2, l_2^2, (l_1 - l_2 - p_1 + p_2)^2 - m^2,$ $(l_1 - l_2 - p_1)^2, l_1^2 - m^2, (l_1 + p_2)^2, (l_1 - p_1)^2$
fam2	$(l_1 + l_2)^2, l_1^2 - m^2, (l_1 - p_1)^2, (l_1 + p_2)^2,$ $l_2^2 - m^2, (l_2 + p_1)^2, (l_2 - p_2)^2$
fam3	$(l_1 + l_2 - p_1 + p_2)^2, l_1^2 - m^2, (l_1 - p_1)^2,$ $(l_1 + p_2)^2, l_2^2 - m^2, (l_2 + p_2)^2, (l_2 - p_1)^2$
fam4	$(l_2 + p_1)^2 - m^2, l_2^2, (l_1 - l_2 - p_1 - p_2)^2 - m^2,$ $(l_1 - l_2 - p_1)^2, l_1^2 - m^2, (l_1 - p_2)^2, (l_1 - p_1)^2$
fam5	$(l_1 + l_2 - p_1 - p_2)^2, l_1^2 - m^2, (l_1 - p_1)^2,$ $(l_1 - p_2)^2, l_2^2 - m^2, (l_2 - p_2)^2, (l_2 - p_1)^2$
fam6	$l_1^2 - m^2, l_2^2, (l_2 - p_1)^2, (l_1 - p_2)^2,$ $(l_1 - l_2 - p_2)^2, (l_1 - l_2 + p_1 - p_2)^2, (l_1 - l_2)^2$

Table 2: The five generic integral families appearing in the forward Compton scattering amplitudes. Families 4 and 5 are obtained from families 1 and 3, respectively, by the crossing $p_2 \rightarrow -p_2$.

We organize the scalar integrals into integral families, each defined by a linearly independent set of propagators. To map a given integral onto one of these families efficiently, we employ the method of Ref. [43] and implement its algorithms into a computer code, which identifies equivalent propagator sets through momentum shifts. In formulation of [43], a momentum shift corresponds to a permutation of the Feynman parameters in the underlying Feynman graph polynomial. Our code systematically searches for such permutations, mapping all scalar integrals onto the six families listed in Tab. 2. Finally, we reduce the integrals belonging to each family to a set of master integrals using integration-by-parts (IBPs) identities generated by REDUZE [52], obtaining 111 generic master integrals in total. The amplitude then takes the form

$$\mathcal{M}_l(Q^2, m^2, s; d) = \sum_k r_{lk}(Q^2, m^2, s; d) j_k, \quad (2.18)$$

where l labels the form factor (cf. Eq. (2.11)), r_{lk} are rational functions of the kinematic variables and d , and j_k denote the master integrals.

Equation (2.18) decomposes the amplitude into rational coefficient functions and master integrals, rendering its analytic structure transparent. The rational coefficients are straightforward, except for the Born-cut diagrams, where the imaginary part is defined by cutting only the massless propagator $1/(s + i0)$, which appears entangled with IBP coefficients. To access the relevant analytic properties, one must consider the real and imaginary parts of the generic master integrals j_k , as discussed in Refs. [44, 53–55]. In this work, we do not compute the full generic integrals; instead, we extract specific contributions to their real and imaginary parts using cut-based techniques, as explained below.

3 Computation of master integrals

The computation of coefficient functions requires the integration of dimensionally regulated scalar integrals over the kinematic domain defined by the phase-space constraints of the final states. We categorize these integrals into four distinct sets based on their cut structure: the I- and II-systems (real-real), III-system (mixed real-real and real-virtual), and the IV-system (fully virtual). Given the similarity, in the real-radiation case, between differential equation systems, we focus on providing full computational details for the I-system, while presenting the II- and III-systems mainly to highlight essential differences and to enable reproduction of our results. The IV-system is treated separately, though many aspects of the calculations discussed for the real-radiation case apply readily to the virtual one.

3.1 Cut based approach to differential equations

The differential equation method represents a standard approach for evaluating Feynman integrals [56, 57]. To derive the differential equations (DEQs), we begin by differentiating the Feynman integrals with respect to each kinematic variable in Eq. (2.7). Using IBPs computed earlier, we express the differentiated integrals in terms of our chosen basis, obtaining a system of coupled differential equations of the form

$$\frac{\partial \mathbf{j}}{\partial x_i} = M_i \cdot \mathbf{j}, \quad (3.1)$$

where the kinematic variables have been rendered dimensionless: $x_1 = s/Q^2$, $x_2 = m^2/Q^2$. The vector $\mathbf{j} = (j_1, j_2, \dots, j_{111})$ represents the *generic* master integrals in the chosen basis. Here, the matrices $M_i = M_i(x_1, x_2; \epsilon)$ for $i = 1, 2$ contain rational functions of the dimensionless kinematic variables and the dimensional regularization parameter ϵ . These matrices encode all analytic properties of the integrals, including physical thresholds, singular structures, and branch cuts. Crucially, they also fully characterize the *cuts* of the integrals.

The imaginary part of a generic integral is given by the cutting equations [45, 58]

$$\text{Im } j_k = j_k - (j_k)^* \doteq \theta(x_1 - 4x_2) j_{k,RRB} + \theta(x_1 - x_2) j_{k,RRC} + \theta(x_1) (j_{k,RRA} + j_{k,RV}), \quad (3.2)$$

where we use the labels of the corresponding cut Feynman diagrams (RRB, RRC, RRA, RV from Tab. 1) as indices for the cut master integrals $j_{k,i}$ to emphasize their correspondence;

these distinct mathematical objects should not be confused with each other. Here, $(j_k)^*$ denotes the complex conjugate integral. The θ -functions encode the physical thresholds for particle production. The cut integrals in Eq. (3.2) are obtained by setting the relevant propagators on-shell via the replacement

$$\frac{1}{D_i} = \frac{1}{L_i^2 - M_i^2 + i0} \rightarrow \delta^+(L_i^2 - M_i^2) = \delta(L_i^2 - M_i^2) \theta(L_i^0), \quad (3.3)$$

where $\delta(x)$ is the Dirac delta function.

To identify which propagators must be put on-shell for a given cut, the graph-theoretic approach outlined in the previous section is employed. For each master integral, the corresponding graph is constructed, its weighted adjacency matrix is formed, and it is processed with the same algorithms. The results are presented in Tab. 3, which lists the sets of propagator indices (from the families in Tab. 2) that must be placed on-shell for each cut.

We now apply the technical ingredients presented above to organize the calculation:

1. For the I-cut ($I \equiv \text{RRB}$), we enforce the corresponding on-shell conditions from Eq. (3.3) within the generic system of Eq. (3.1), using the mapping provided in Tab. 3. This produces a reduced differential system

$$\frac{\partial \mathbf{j}_I}{\partial x_i} = M_i^I \cdot \mathbf{j}_I, \quad (3.4)$$

where $\mathbf{j}_I = (j_{I,1}, \dots, j_{I,27})$ are the master integrals for the I-cut. The matrices M_i^I are obtained by removing from M_i the rows and columns corresponding to integrals that do not admit this specific cut.

2. Similar to the previous case, we discard generic j that do not possess the RRC cut. Consequently, we obtain the second reduced differential system

$$\frac{\partial \mathbf{j}_{II}}{\partial x_i} = M_i^{II} \cdot \mathbf{j}_{II}, \quad (3.5)$$

where $\mathbf{j}_{II} = (j_{II,1}, \dots, j_{II,8})$ are the master integrals for the II-cut. The matrices M_i^{II} are obtained in the same manner as in the case of I-system.

3. For the III-system, we consider contributions in the kinematic region defined by $0 < x_1 < x_2$, forbidding the I and II cuts. The relevant contributions arise from the union of the RRA and RV cuts, i.e., $III \equiv \text{RRA} \cup \text{RV}$. We therefore select the subset of generic master integrals whose imaginary part receives contributions from these cuts within this kinematic domain. This leads to the system

$$\frac{\partial \mathbf{j}_{III}}{\partial x_i} = M_i^{III} \cdot \mathbf{j}_{III}, \quad (3.6)$$

where $\mathbf{j}_{III} = (j_{III,1}, \dots, j_{III,32})$ comprises the relevant generic master integrals. The system is defined implicitly by the kinematic restriction, rather than by enforcing a specific on-shell condition.

Integrating the differential equations (3.4, 3.5, 3.6) gives the phase-space master integrals required for the real-radiation contributions to the coefficient functions in Eq. (2.13) (e.g. RRA, RRB, RRC, and RV).

The integrals corresponding to the virtual cut in Tab. 1 are also derived from the generic differential system of Eq. (3.1). However, the cut-based method used for the real-radiation case above cannot be applied directly. In Feynman diagrams with the VV cut, the massless quark propagator $1/(x_1 + i0)$ mixes with coefficients from the IBP reduction, preventing a straightforward application of the on-shell prescription. Consequently, at the level of scalar integrals, no direct virtual cut exists. Instead, we identify the virtual contribution by selecting Feynman diagrams with the virtual cut VV, collecting the master integrals appearing in their amplitudes, and discarding the others, obtaining:

$$\frac{\partial \mathbf{j}_{\text{IV}}}{\partial x_i} = M_i^{\text{IV}} \cdot \mathbf{j}_{\text{IV}}, \quad (3.7)$$

where M_i^{IV} is a 41×41 matrix derived from the generic one in Eq. (3.1), and the vector \mathbf{j}_{IV} contains the generic integrals needed for the virtual contribution. These integrals are then further processed: as we demonstrate later, it suffices to study the real part of the IV-system in the asymptotic limit $s \rightarrow 0$ and extract the leading term of the corresponding expansion.

Finally, the canonical form of differential equations introduced by Henn [59] provides significant computational advantages. For a given integral family k , the canonical differential equation reads

$$\frac{\partial \mathbf{J}_k}{\partial y_i} = \epsilon S_i^k \mathbf{J}_k, \quad (3.8)$$

and can be obtained through a gauge transformation

$$\begin{aligned} \mathbf{j}_k &= T_k \mathbf{J}_k, \\ S_i^k &= T_k^{-1} \cdot M_i^k \cdot T_k - T_k^{-1} \cdot \partial_{y_i} T_k. \end{aligned} \quad (3.9)$$

Here, \mathbf{j}_k denotes the vector of Laporta master integrals discussed previously, while \mathbf{J}_k represents the vector of canonical master integrals for $k = \text{I, II, III}$. The transformation matrices T_k convert the original ϵ -dependent matrices $M_i^k = M_i^k(y_1, y_2; \epsilon)$ into canonical matrices $S_i^k = S_i^k(y_1, y_2)$ that are independent of the dimensional regularization parameter. The new kinematic variables y_1 and y_2 are introduced later.

The canonical form offers two key advantages. First, the general solution can be expressed compactly as a path-ordered exponential

$$\mathbf{J}_k = \text{P exp} \left(\epsilon \int_{\gamma} \sum_{k=1,2} S_k \cdot dy_k \right), \quad (3.10)$$

where P is the path-ordering operator and γ specifies the integration contour. Second, it allows a straightforward expansion in the $\epsilon \rightarrow 0$ limit, for instance, via Picard iteration. Thus, the problem of solving the differential equations reduces to finding the transformations T that bring them into this canonical form.

3.2 Real-radiation: canonical transformations

The construction of appropriate transformations that bring the given system of DEQs to canonical form presents considerable challenges and requires a careful analysis of the intricate singular structure of the M_i^k matrices. To address this issue, we employ the framework implemented in the **Mathematica** package **Libra** [60], which provides semi-automatic tools for obtaining canonical forms. The package implements algorithms based on balance transformations and the systematic reduction of the Poincaré rank of the DEQs, ultimately ensuring that all singularities are Fuchsian [61].

A notable feature of **Libra** is the possibility, within limitations, to find balance transformations involving algebraic extensions

$$T_{i,j} = R_1(x) + u(x)R_2(x),$$

where $R_{1,2}$ are rational functions and u satisfies $u^2 = q(x)$, where $q(x)$ is a polynomial. Such extensions in the transformation matrix are often related to massive particles in the scattering process, as heavy-pair production.

Transformations of the system (3.1) would have involved three square roots, defined by:

$$\begin{aligned} u_1^2 - (x_1^2 + 2x_1(1 - x_2) + (1 + x_2)^2) &= 0, \\ (x_1 + 2(1 + x_2))u_2^2 - x_1 + 2(1 - x_2) &= 0, \\ (x_1 - 4x_2)u_3^2 - x_1 &= 0. \end{aligned} \tag{3.11}$$

By imposing on-shellness and other constraints as previously detailed, u_2 is completely removed from our systems, while the algebraic extensions (roots) u_1 and u_3 remain and still pose significant computational challenges.

To manage the remaining roots, we implement the variable transformation

$$x_1 \rightarrow \frac{y_1}{(1 - y_1)(1 - y_2)}, \quad x_2 \rightarrow \frac{y_2}{(1 - y_1)(1 - y_2)}, \tag{3.12}$$

which rationalizes u_1 , leaving only u_3 in the system M^I . The resulting differential equations in the y -variables read

$$\frac{\partial \mathbf{j}_k}{\partial y_i} = M_i^k \cdot \mathbf{j}_k, \tag{3.13}$$

where now $M_i^k = M_i^k(y_1, y_2)$, $k = 1, 2, 3$ and $\mathbf{j}_k = \mathbf{j}_k(y_1, y_2)$.

This variable change is chosen to achieve three goals: parametrizing the soft limit $x_1 \rightarrow 0$ in a convenient form (discussed later), not increasing the complexity of the coefficient matrices, and reducing the algebraic complexity of the transformations. Consequently, after applying this change, no further technical obstacles prevent us from obtaining the

ϵ -form of Eq. (3.13). The canonical differential equation matrices in Fuchsian form read⁵

$$\begin{aligned} S_k^I(y_1, y_2) &= \sum_i \frac{S_{ik}^I}{y_k - a_{k,i}^I} + u(y_1, y_2) \sum_i \frac{S_{ik}^Q}{y_k - a_{k,i}^Q}, \\ S_k^{II}(y_1, y_2) &= \sum_i \frac{S_{ik}^{II}}{y_k - a_{k,i}^{II}}, \\ S_k^{III}(y_1, y_2) &= \sum_i \frac{S_{ik}^{III}}{y_k - a_{k,i}^{III}}, \end{aligned} \quad (3.14)$$

where the S_k^l are constant matrices, $u_3 \equiv u = \sqrt{y_1/(y_1 - 4y_2)}$, and the a_i^l denote the locations of singularities in kinematic space, often referred to as *letters* in the literature. A set of letters constitutes an *alphabet* of the corresponding DEQ system. The relevant alphabets are presented in Eqs. (B.1)–(B.4).

3.3 Real-radiation: integration

As discussed previously, the canonical form of the differential equations admits an exponential solution with ϵ appearing in a fully factorized form. We expand the exponential solution in Eq. (3.10) as a series around $\epsilon = 0$, using the canonical matrices from Eq. (3.14). The practical implementation of this expansion employs Picard iteration.⁶ The solution for the i -system on the path $\gamma_1^i : [0, y_{k_i}]$ is obtained by successive iterations of the corresponding matrix $S_{k_i}^i$, where $i = I, II, III$ and $\{k_I = 2, k_{II} = 2, k_{III} = 1\}$, as follows:

$$\mathbf{J}_i = \sum_{n=0}^{N_i} \epsilon^n \mathbf{J}_i^{(n)}, \quad (3.15)$$

with

$$\mathbf{J}_i^{(n)} = \tilde{\mathbf{C}}_{\gamma_1^i}^{(n)} + \int_0^{y_{k_i}} S_{k_i}^i(t) \circ \mathbf{J}_i^{(n-1)}(t) dt, \quad (3.16)$$

where \circ denotes path-ordered matrix multiplication along γ_1^i . We employ a compact notation for the S -matrices and other tensors, showing only the active integration variable (i.e., $t \equiv (y_1, t)$ for $i = I, II$ and $t \equiv (t, y_2)$ for $i = III$, with the inactive coordinate held fixed). Here, for $n = 0, 1, 2, \dots$, $\tilde{\mathbf{C}}_{\gamma_1^i}^{(n)}$ are integration constants and $\mathbf{J}_i^{(0)} \equiv \tilde{\mathbf{C}}_{\gamma_1^i}^{(0)}$. It is sufficient to expand up to order $N_i = 5$ to capture all finite contributions in the coefficient functions, since the highest pole of typical four-point NNLO corrections does not exceed $\mathcal{O}(\epsilon^{-4})$ [62].

The iterated integral structure of the evolution matrix is made explicit by re-expanding the Picard iterates. For the straight-line path γ_1^i we have

$$\mathbf{J}_i = \mathbf{U}_{\gamma_1^i} \cdot \mathbf{C}_{\gamma_1^i}, \quad (3.17)$$

⁵Given that our system involves algebraic extensions, we consider singularities as Fuchsian provided no subsequent variable transformation increases their Poincaré rank. We thank M. Bonetti for private conversations on this matter.

⁶Picard iteration reproduces the formal solution of Eq. (3.10) when summed to all orders in ϵ , provided the matrix is in block-triangular form.

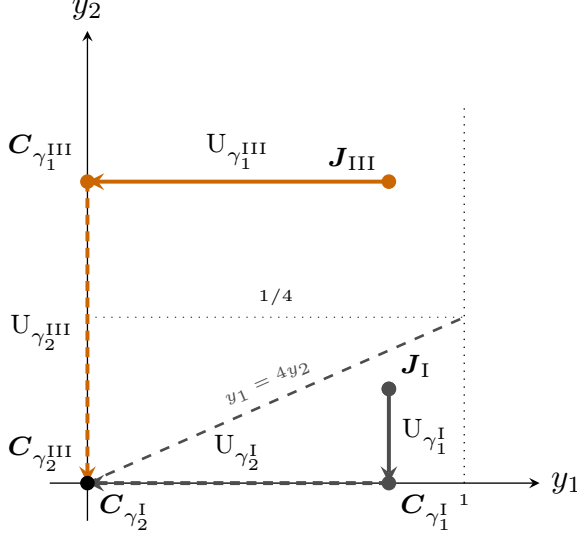


Figure 2: Integration paths in the (y_1, y_2) plane specific to the systems defined in the text. The I- and II-systems follow the same integration contour, differing only in their initial phase-space points.

where the evolution matrix $U_{\gamma_1^i}$ is given by the series

$$U_{\gamma_1^i} = \mathbb{1} + \sum_{n \geq 1} \epsilon^n S_{(n)}^i(y_1, y_2), \quad (3.18)$$

$$S_{(n)}^i(y_1, y_2) = \int_0^{y_{k_i}} dt_n \int_0^{t_n} dt_{n-1} \cdots \int_0^{t_2} dt_1 S_{k_i}^i(t_n) \circ S_{k_i}^i(t_{n-1}) \circ \cdots \circ S_{k_i}^i(t_1),$$

with $\mathbb{1}$ the identity matrix and the matrices in the integrand are path-ordered along γ_1^i .

We demonstrate the method for determining integration constants using the I-system as an example [63]. To obtain $\mathbf{C}_{\gamma_1^i} = \mathbf{C}_{\gamma_1^i}(y_1)$, we construct the corresponding differential system in two steps.

First, because the matrices S_2^i are Fuchsian, the evolution matrix $U_{\gamma_1^i}$ from Eq. (3.17) admits near $y_2 = 0$ a generalized series expansion, whose coefficients are determined via the Frobenius method [60, 64, 65]. For the I-system, this expansion takes the form

$$U_{\gamma_1^i}(y_1, y_2) = \sum_{\lambda \in S} (y_2)^\lambda \sum_{n=0}^{\infty} \sum_{k=0}^{K_\lambda} A_{n+\lambda, k} y_2^n \log^k(y_2), \quad (3.19)$$

where $A_{n+\lambda, k} = A_{n+\lambda, k}(y_1, \epsilon)$ are rational function matrices. The exponents λ and their multiplicities K_λ are obtained from the corresponding indicial polynomial as prescribed in Ref. [64].

Second, substituting this series expansion into the canonical y_2 -system (with the DEQ matrices provided in Eq. (3.14)) gives

$$\frac{\partial \mathbf{C}_{\gamma_1^i}}{\partial y_1} = \epsilon \tilde{S}^i(y_1) \cdot \mathbf{C}_{\gamma_1^i}, \quad \tilde{S}^i(y_1) = \sum_i \frac{\tilde{S}_i^i}{y_1 - b_i^i}. \quad (3.20)$$

Here, \tilde{S}^I is a new matrix derived from the canonical ones in Eq. (3.14), with its alphabet defined in Eq. (B.4). Provided the original system is in canonical form, this two-step procedure preserves the ϵ -form of the differential equations. Consequently, they can be solved using the same methods applied to the y_2 -system.

Integrating Eq. (3.20) along the γ_2^I path gives

$$\begin{aligned} \mathbf{C}_{\gamma_2^I} &= \mathbf{U}_{\gamma_2^I}^I \cdot \mathbf{C}_{\gamma_2^I} = \left(\mathbf{1} + \sum_{n \geq 1} \epsilon^n \tilde{S}_n^I(y_1) \right) \cdot \mathbf{C}_{\gamma_2^I}, \\ \tilde{S}_n^I(y_1) &= \int_0^{y_1} dt_n \int_0^{t_n} dt_{n-1} \cdots \int_0^{t_2} dt_1 \tilde{S}^I(t_n) \circ \tilde{S}^I(t_{n-1}) \circ \cdots \circ \tilde{S}^I(t_1), \end{aligned} \quad (3.21)$$

where \circ now denotes path-ordering along γ_2^I . The path $\gamma_2^I : [0, y_1]$ connects the solution at $\mathbf{y} = (y_1, 0)$ from Eq. (3.18) to the origin, where the integration constants $\mathbf{C}_{\gamma_2^I}$ are fixed via the PSLQ method (discussed later). Applying the same procedure in the order specific to the II, III systems produces the derived matrices \tilde{S}^{II} and \tilde{S}^{III} with alphabet defined in Eqs. (B.6, B.7), respectively; the corresponding differential equations are then integrated analogously to Eq. (3.21).

The matrix elements in Eqs. (3.18) and (3.21) are iterated integrals defined as [66]:

$$G(a_1, \dots, a_n; y_k) := \int_0^{y_k} \frac{d^* t_1}{t_1 - a_1} \int_0^{t_1} \frac{d^* t_2}{t_2 - a_2} \cdots \int_0^{t_{n-1}} \frac{d^* t_n}{t_n - a_n}, \quad (3.22)$$

with $G(\cdot; y_k) := 1$. We adopt the notation of Ref. [67], where the integration measure $d^* t$ is generalized to include both rational and algebraic cases:

$$d^* t = \begin{cases} dt & (\text{rational}) \\ u dt & (\text{algebraic}) \end{cases}, \quad u = \sqrt{y_1/(y_1 - 4y_2)}. \quad (3.23)$$

When all measures are rational, Eq. (3.22) coincides with the standard definition of Goncharov polylogarithms [68]. The algebraic case, which appears exclusively in $\mathbf{U}_{\gamma_2^I}$, requires additional treatment. We apply the transformation

$$t_i \rightarrow y_1 \frac{(u_i^2 - 1)}{4u_i^2}, \quad (3.24)$$

to rationalize the measure. After simplifying the resulting integrand, the expression again reduces to Goncharov polylogarithms, but with a modified alphabet given in Eq. (B.6).

3.4 Virtual: canonical transformations and integration

Virtual integrals require special treatment because we cannot isolate virtual cuts at the scalar integral level, as discussed in Sec. 3.1. The complication arises because the would-be-cut massless quark propagator becomes entangled with IBP coefficients, preventing direct extraction of the desired cut.

Our systematic solution retains the original scalar propagator structure by exploiting how virtual contributions originate from the Feynman propagator's analytic structure.

Specifically, the imaginary part of the amplitude (Eq. (2.18)) stems, in the virtual case, from rational coefficients through the on-shell condition defined in Eq. (3.3)

$$\frac{1}{y_1 + i0} \rightarrow -i\pi\delta(y_1). \quad (3.25)$$

Consequently, only the real part of \mathbf{j}_{IV} near $y_1 = 0$ must be computed. For clarity, we apply this substitution only when the pole $1/y_1$ becomes manifest in the amplitude, after virtual integrals are substituted in Eq. (2.18).

To achieve this, we first regularize M_i^{IV} from Eq. (3.13) at $y_1 = 0$ by applying the balance transformations obtained using **Libra**, which reduce the $1/y_1$ pole to first order. As in the previous section, generalized series solutions can be obtained via the Frobenius method near simple poles. Eventually, for the Laporta master integrals, we obtain the solution near $y_1 = 0$

$$\mathbf{j}_{\text{IV}} = \mathbf{U}_{\gamma_1^{\text{IV}}} \cdot \mathbf{c}_{\gamma_1^{\text{IV}}}, \quad (3.26)$$

where the path γ_1^{IV} matches that of the III-system. The vector $\mathbf{c}_{\gamma_1^{\text{IV}}} = \mathbf{c}_{\gamma_1^{\text{IV}}}(y_2)$ contains the integration constants for the generic integrals near $y_1 = 0$. For the virtual contribution, we retain only the $\lambda = 0$ solution from the full expansion (cf. Eq. (3.19)), since the other solutions do not contribute to the virtual integrals. Thus, the expansion reduces to the form

$$\mathbf{U}_{\gamma_1^{\text{IV}}}(y_1, y_2) = \sum_{n=0}^N A_{n,k} y_1^n + \mathcal{O}(y_1^{N+1}), \quad (3.27)$$

which we truncate at order N . This truncation retains only the simple-pole contribution in y_1 at the amplitude level; we have verified explicitly that higher-order poles cancel. Terms with $\lambda \neq 0$ would lead to integrands proportional to

$$\delta(y_1) (y_1)^\lambda \log^k(y_1), \quad (3.28)$$

which, upon imposing the δ -constraint, vanish identically, provided that $\lambda \propto \text{Re}(\epsilon) < 0$. Here, we obtain 16 independent integration constants in $\mathbf{c}_{\gamma_1^{\text{IV}}}$, while the remaining 26 boundary conditions of the original system are discarded, as they do not contribute to the virtual part.

Similar to the real-radiation case, we derive differential equations for the virtual integration constants by substituting Eq. (3.27) into the corresponding y_2 -equations from Eq. (3.13). This produces a simple single-variable system, that is transformed to ϵ -form using the procedure detailed in Sec. 3.2

$$\frac{\partial \mathbf{C}_{\gamma_1^{\text{IV}}}}{\partial y_2} = \epsilon \tilde{S}^{\text{IV}}(y_2) \cdot \mathbf{C}_{\gamma_1^{\text{IV}}}, \quad \tilde{S}^{\text{IV}}(y_2) = \sum_i \frac{\tilde{S}_i^{\text{IV}}}{y_2 - b_i^{\text{IV}}}. \quad (3.29)$$

The notation is kept consistent with the real-radiation case. The virtual system's alphabet is given in Eq. (B.8).

Integration proceeds analogously to the real-radiation case using the Picard iteration method from Sec. 3.3 (Eq. (3.21)).

3.5 Boundary conditions

The differential equations for the I-, II-, III-, and IV-systems have been integrated analytically up to integration constants. This section describes the numerical determination of these constants. These numerically determined constants are subsequently employed in Sec. 3.3 to obtain the fully normalized, uniformly transcendental expressions for the master integrals

We determine the constants using the PSLQ algorithm [69], which identifies rational linear combinations of basis constants matching high-precision numerical values. The relevant basis consists of constants of transcendental weight up to five [59]:

$$\pi^n, \zeta_n, \log^n(2), \text{Li}_n(1/2), \quad n = 1, 2, 3, 4, 5, \quad (3.30)$$

and their products, where weight adds under multiplication. The weight corresponds to the depth of iterated integration in the functions' definition (cf. Eq. (3.22)). The constants above admit known definitions in terms of iterated integrals from which their weights can be determined.

Our final expressions are required to be in *uniformly transcendental* (UT) form: all terms at order ϵ^n have weight exactly n . The canonical basis alone does not guarantee this which necessitates an appropriate ϵ -dependent normalization. We determine the normalization factors f_i by analyzing the simplest integral topology within each system. We transform the simplest Laporta master integrals, computed via parametric integration, to the canonical basis. Extracting their boundary conditions from the generalized series solutions (Sec. 3.3) produces constants. Demanding that the resulting constants be of pure weight determines the normalization factor in front of the integral measure

$$f_i S_\epsilon^2 \int \frac{d^d l_1}{(2\pi)^{d'}} \frac{d^d l_2}{(2\pi)^{d'}}, \quad (3.31)$$

with $d' = d - 1$ for the I, II systems (cut integrals) and $d' = d$ otherwise. The factor f_i for each system is given in Eq. (B.11) of the appendix. The spherical factor S_ϵ is defined as

$$S_\epsilon = \exp(\epsilon(\ln 4\pi - \gamma_E)), \quad (3.32)$$

where $\gamma_E \approx 0.577\dots$ is the Euler–Mascheroni constant.

High-precision numerical values for the Laporta integrals \mathbf{j} are obtained using `AMFlow` [70], which implements the auxiliary mass flow method and supports arbitrary-precision arithmetic (typically $\mathcal{O}(300)$ digits). The kinematics are chosen according to the cut prescription discussed in Sec. 3.1.

- I-system: $y_1 > 4y_2, y_2 > 0$ (denominators put on-shell).
- II-system: $y_1 > y_2, y_2 > 0$ (denominators put on-shell).
- III-system: $y_1 < y_2, y_2 > 0$ (generic integrals; keep imaginary part).
- IV-system (virtual): $y_1 = 0, y_2 > 0$ (boundary from Eq. (3.27)).

The constants are extracted via the following procedure:

1. Compute the Laporta integrals \mathbf{j} numerically at the chosen kinematic points.
2. Apply the inverse balance transformation together with the normalization factors of Eq. (3.31) to convert the numerical \mathbf{j} to the normalized UT basis \mathbf{J} .
3. Evaluate the analytic solutions for \mathbf{J} (Sec. 3.3) to the same high precision using `PolyLogTools` [71] (which calls `GiNaC` [72]).
4. Subtract the analytic result from the numerical one. All functional dependence cancels, leaving only constants.
5. Use the PSLQ algorithm to fit each derived numerical value to a linear combination of transcendental constants presented in Eq. (3.30).

We conclude this section by outlining how our results were verified. First, we note that the fitting procedure already guarantees the correctness of the evolution part. Indeed, if the analytic solution were incorrect, the resulting numerical constants would not match the transcendental basis defined in Eq. (3.30), and the PSLQ algorithm would fail to produce a fit.

As a further check, we evaluated our final analytic solutions at kinematic points different from those used in the fitting step, and compared them against corresponding numerical results from `AMFlow`, finding full agreement within specified accuracy reaching 300 digits.

4 Results

Here we present the main result of this paper: the renormalized coefficient functions through $\mathcal{O}(\alpha_s^2)$. First, we briefly discuss UV renormalization and the regularization of IR singularities. We then detail the exact structure of the partonic structure functions at each perturbative order. Complete analytic expressions are provided as auxiliary files with this publication.

4.1 Renormalization

The forward Compton scattering amplitude from Eq. (2.16) admits a perturbative expansion in the bare strong coupling constant $\alpha_{s,0}$

$$\mathcal{M}_0^{\mu\nu} = \mathcal{M}_0^{(0),\mu\nu} + a_0 \mathcal{M}_0^{(1),\mu\nu} + a_0^2 \mathcal{M}_0^{(2),\mu\nu} + \mathcal{O}(a_0^3), \quad (4.1)$$

where $a_0 = \alpha_{s,0}/2\pi$. The terms $\mathcal{M}_0^{(k),\mu\nu}$ with $k = 0, 1, 2$ denote the respective perturbative contributions; the leftmost subscript “0” indicates an unrenormalized quantity. This expansion matches, order by order in a_0 , the perturbative structure of the unrenormalized coefficient functions that enter Eq. (2.5). Below we summarize the renormalization constants needed to obtain finite quantities.

The choice of renormalization scheme for the strong coupling constant requires careful consideration. While one could, in principle, use the $\overline{\text{MS}}$ scheme, the resulting DGLAP

evolution becomes rather involved due to heavy-quark self-energy diagrams entering the corresponding equations. It is preferable to subtract the heavy-quark contribution at zero momentum [73]. We therefore adopt the decoupling scheme, following Refs. [18, 19, 74, 75]: here, the light flavors are treated in $\overline{\text{MS}}$, while the heavy quark decouples from the evolution equations.

Within this scheme, the coupling renormalization is given by

$$a = Z_g^2 a_0 = a(Q^2) \left(1 + a(Q^2) \left(-\frac{\beta_0}{2\epsilon} - n_H \frac{\beta_{0,Q}}{2\epsilon} \left(\frac{m^2}{Q^2} \right)^{-\epsilon} \left(1 + \frac{1}{2} \epsilon^2 \frac{\pi^2}{6} \right) \right) \right), \quad (4.2)$$

where the lowest-order beta functions are

$$\beta_0 = \frac{11}{3} C_A - \frac{4}{3} T_R n_L, \quad (4.3)$$

$$\beta_{0,Q} = -\frac{4}{3} T_R. \quad (4.4)$$

Here, $n_L = 3$ and $n_H = 1$ denote the number of light and heavy quarks, respectively, and the $\mathfrak{su}(N)$ color factors are $C_F = (N_c^2 - 1)/2N_c$, $C_A = N_c$, $T_R = 1/2$ with $N_c = 3$. The term proportional to n_H modifies the renormalization constant Z_g by introducing a mass-dependent finite counterterm. This modifies the $1/\epsilon$ pole structure in the Callan-Symanzik equation, resulting in a beta function from which the heavy-quark contribution is removed. Using this scheme ensures that only the n_L light flavors participate in the DGLAP evolution.

The renormalized amplitude reads

$$\mathcal{M}^{\mu\nu} = (Z_{2,Q}^{\text{OS}} \mathcal{M}_0^{\mu\nu}) \Bigg|_{\substack{a_0 \rightarrow Z_g^2 a, \\ m_0 \rightarrow Z_m^{\text{OS}} m.}} = \mathcal{M}^{(0),\mu\nu} + a \mathcal{M}^{(1),\mu\nu} + a^2 \mathcal{M}^{(2),\mu\nu} + \mathcal{O}(a^3), \quad (4.5)$$

where $Z_{2,Q}^{\text{OS}}$ and Z_m^{OS} are the on-shell renormalization constants taken from Ref. [76]. We have verified that at this perturbative order the choice of $Z_{2,Q}$ does not affect the coefficient functions provided the pole mass m is used. We believe that this is due to “the S -matrix being the same for renormalized as for unrenormalized Green functions”, as follows from the discussion in Ref. [77]. The renormalization scheme for the operator matrix elements that define PDFs must, however, be consistent with our choice.

The finite flavor-stripped coefficient functions inherit the perturbative expansion of the renormalized amplitude

$$C_{j,n}(y_1, y_2, Q^2) = \delta(y_1) + a C_{j,n}^{(1)}(y_1, y_2, Q^2) + a^2 C_{j,n}^{(2)}(y_1, y_2, Q^2) + \mathcal{O}(a^3), \quad (4.6)$$

where

$$C_{j,n}^{(i)} = \frac{\mathcal{N}_j}{\mathcal{B}_j} \text{Im} \mathcal{M}_{j,n}^{(i)}. \quad (4.7)$$

Here, the normalization factors \mathcal{N}_j are defined in Eq. (2.15) and \mathcal{B}_j are the Born coefficient functions, presented later. This normalization choice implies $C_{j,n}^{(0)} \equiv \delta(y_1)$. The imaginary parts $\text{Im} \mathcal{M}_{j,n}^{(i)}$ are extracted using the cut-based methods described in Secs. (2.2, 3.1).

Finally, we discuss the impact of the renormalization scheme on the coupling, with coefficient functions obtained at the factorization/renormalization point $\mu_F^2 = \mu_R^2 = Q^2$, i.e., $C_{j,n}^{(i)} \equiv C_{j,n}^{(i)}(\mu_R^2 = Q^2)$. To restore their full scale dependence, we use the fact that the hadronic structure functions in Eq. (2.13) are independent of the renormalization scale. Within our scheme, the scale dependence is straightforward to derive; we present the result without reproducing the full evolution equations

$$C_{j,n} = \delta(y_1) + a(\mu_R^2) C_{j,n}^{(1)}(Q^2) + a^2(\mu_R^2) \left(C_{j,n}^{(2)}(Q^2) + \beta_0 \log\left(\frac{\mu_F^2}{Q^2}\right) C_{j,n}^{(1)}(Q^2) \right) + \mathcal{O}(a^3), \quad (4.8)$$

where, to restore the dependence on the factorization scale, we have solved the renormalization group equation for α_s to express $\alpha_s(\mu_F^2)$ in terms of $\alpha_s(\mu_R^2)$. Here, β_0 (Eq. (4.3)) corresponds to n_L light flavors.

4.2 Isolating soft contribution

In Sec. 2.2, we used dimensional regularization to regulate both UV and IR divergences in the forward Compton scattering amplitude up to $\mathcal{O}(\alpha_s^2)$. At this order, the corresponding loop integrals produce poles up to $1/\epsilon^4$ at two loops [62]. While UV divergences are removed by renormalization in the previous section, the cancellation of IR poles, in general, requires a systematic analysis of phase-space integrals, as different kinematic configurations produce characteristic ϵ -pole structures. Here, we only need to focus on the soft limit $y_1 \rightarrow 0$ of the coefficient functions.

Dimensional regularization correctly handles soft-collinear divergences in the $y_1 \rightarrow 0$ limit. However, our treatment of the $\epsilon \rightarrow 0$ limit during master integral evaluation disturbs their proper behavior near $y_1 = 0$, which in turn affects the partonic structure functions in the soft region. This becomes evident from the asymptotic expansion of the master integrals \mathbf{J}_{III} in the soft limit

$$A_{y_1} [\mathbf{J}_{\text{III}}] = \sum_{\lambda \in S} y_1^\lambda \sum_{n=0}^N \sum_{k=0}^{K_\lambda} y_1^n \log^k(y_1) A_{n+\lambda,k}^{\text{III}} \cdot \mathbf{C}_{\gamma_1^{\text{III}}}, \quad (4.9)$$

with exponent set $S = \{-\epsilon, -2\epsilon, -3\epsilon, -4\epsilon\}$. Here, A_{y_1} denotes the truncated generalized series solution from Sec. 3.3. This expansion makes the integrals' singular structure explicit, ensuring that physical soft singularities are properly regulated once inserted into the hadronic integral (cf. Eq. (2.13)).

The appearance of $y_1^{-a-b\epsilon}$ divergences for $a, b > 0$, which enter the hadronic structure functions through Eq.(4.9), signals the non-commutativity of the limits $y_1 \rightarrow 0$ and $\epsilon \rightarrow 0$, requiring a careful ordering. Following Ref. [45], we restore the correct soft behavior via the regularization prescription

$$\mathbf{J}_{\text{III}} \rightarrow \mathbf{J}_{\text{III}} - T_{y_1} [\mathbf{J}_{\text{III}}] + A_{y_1} [\mathbf{J}_{\text{III}}], \quad (4.10)$$

for the III-system. Here, T_{y_1} is the truncated Taylor expansion around $y_1 = 0$. The subtraction of the Taylor expansion removes the incorrect behavior of the scalar integrals

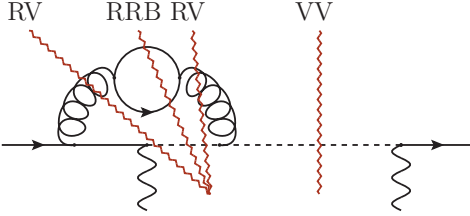


Figure 3: One of the diagrams in which each individual cut (cf. Tab. 1) produces a large triple logarithm.

in the soft limit, while adding back the asymptotic expansion reinstates the correct singular structure. The precise truncation order N is unimportant in practice, provided it is large enough not to affect finite contributions in the coefficient functions.

Applying the prescription in Eq. (4.10) regularizes the corresponding structure functions through the replacement rule

$$\lim_{\Delta \rightarrow 0} \int_{\Delta}^1 dy_1 g y_1^{-a-b\epsilon} = \int_0^1 dy_1 g \left(\frac{\delta(y_1)}{1-a-b\epsilon} + y_1^{1-a} \sum_{k=0} \frac{(-b\epsilon)^k}{k!} \mathcal{D}_k(y_1) \right), \quad (4.11)$$

where Δ is an auxiliary infrared regulator, introduced to properly define the integral on the left-hand side; it completely vanishes as $\Delta \rightarrow 0$, provided that $\text{Re}(\epsilon) < 0$. Here, $g = g(y_1)$ is some properly defined test function. The functions $\mathcal{D}_k(x)$ are *plus-distributions* defined as [78]:

$$\int_0^1 dx g(x) \mathcal{D}_k(x) = \int_0^1 dx \frac{\log^k(x)}{x} (g(x) - g(0)), \quad (4.12)$$

for $k \geq 0$; for $k = -1$ we additionally define $\mathcal{D}_{-1}(x) = \delta(x)$. Through Eq. (4.11), the soft divergences of the amplitude are re-expressed as poles in ϵ , as required.⁷

The RRB and RRC contributions behave differently in the soft region. The phase-space constraint for the heavy quark final state(s), imposed via $\theta(s - 4m^2)$ or $\theta(s - m^2)$ in the convolution integral (Eq. (2.3)), shields it from the massless soft singularity at $s = 0$. The heavy-quark mass thus acts as a natural IR cutoff, allowing a naive ϵ -expansion of the I and II systems.

Although beyond the scope of this work, it is instructive to consider the limit $\frac{m^2}{Q^2} \rightarrow 0$. Convolving PDFs with the RRB coefficient functions produces hadronic functions that diverge as $\log^3(m^2/Q^2)$ in this limit due to Sudakov enhancement [16, 79, 80]. One diagram responsible for this behavior is shown in Fig. 3. The explanation follows Refs. [16, 80]: as m^2/Q^2 decreases, the upper integration boundary in Eq. (2.3) approaches the massless soft singularity at $\xi = 1$, and the virtual gluon producing the heavy-quark pair becomes soft, inducing an additional logarithmic enhancement. However, the sum over all cut diagrams of the type represented in Fig. 3, must cancel these logarithms exactly (cf. Refs. [16, 79, 80]).

⁷To avoid proliferating definitions, we use the same symbol for lower and upper plus-distributions. The position of the regulated divergence can be inferred from the variable context (e.g., ξ , ξ' , or y_1).

To facilitate an analytical demonstration of this cancellation later, we prepare by slightly modifying the regularization procedure for the I-integrals in the soft limit as

$$\mathbf{J}_I \rightarrow \mathbf{J}_I - T_{y_1} \circ A_{y_2} [\mathbf{J}_I] + A_{y_1} \circ A_{y_2} [\mathbf{J}_I]. \quad (4.13)$$

We emphasize that, due to phase-space constraints, the limits $y_1 \rightarrow 0$ and $y_2 \rightarrow 0$ do not commute for the I-system. Applying this prescription to the RRB diagrams gives an asymptotic expansion of the corresponding coefficient functions of the form

$$g = g_0 + g_1 y_2^{-\epsilon} + g_2 y_2^{-2\epsilon} + \mathcal{O}(y_2), \quad (4.14)$$

where $g_l = g_l(y_1)$ for $l = 0, 1, 2$. The coefficients obtained in this way are correctly regulated in the soft $y_1 \rightarrow 0$ limit. The convolution integral for each coefficient can then be written as

$$\begin{aligned} \int_{4y_2}^1 dy_1 g_l(y_1) y_1^{-1-b\epsilon} = \\ \int_0^1 dy_1 g_l(y_1) \left(\delta(y_1) \frac{1 - 4^{-b\epsilon} y_2^{-b\epsilon}}{-b\epsilon} + \sum_{k=0}^{\infty} \frac{(-b\epsilon)^k}{k!} \mathcal{D}_k(y_1) \right) + \mathcal{O}(y_2), \end{aligned} \quad (4.15)$$

where the lower limit in the second term has been set to 0.

A few comments on this result are necessary. In the previously considered case of massless final states (the III-system), an auxiliary infrared regulator Δ is introduced to properly define convolution integrals; this auxiliary regulator vanishes in the $\Delta \rightarrow 0$ limit for $\text{Re}(\epsilon) < 0$. For the RRB cut, however, the lower boundary in Eq. (4.15) is fixed by phase-space constraints and represents an *actual*, not auxiliary, regulator. Consequently, it must be retained in the subsequent analysis of the RRB contribution. The non-commutativity of infrared limits [81] means that applying the auxiliary-regulator limiting procedure here would incorrectly suppress the $y_1^{-a-b\epsilon}$ contribution as $y_2 \rightarrow 0$, generating a spurious $1/\epsilon$ pole in the integrand. The correct procedure is therefore to expand in ϵ *under the integral sign* while keeping y_2 finite but vanishingly small; in this way, the ϵ -pole cancels, and the logarithmically enhanced terms required for a smooth massless limit are produced [81].

4.3 Born coefficient functions

Upon applying the variable change defined in Eq. (3.12), the on-shell condition (cf. Eq. (3.25)) reduces to

$$\delta(s) = \frac{(1 - y_2)}{Q^2} \delta(y_1), \quad (4.16)$$

which, together with Eqs. (2.4) and (2.15), provides the leading order hadron structure functions

$$\begin{aligned} F_1^0(x_B, Q^2) &= |\mathcal{V}_{\text{cs}}|^2 \mathcal{B}_1 f_Q(\eta, Q^2) = \frac{1}{2} S_+ |\mathcal{V}_{\text{cs}}|^2 f_Q(\eta, Q^2), \\ F_2^0(x_B, Q^2) &= |\mathcal{V}_{\text{cs}}|^2 \mathcal{B}_2 f_Q(\eta, Q^2) = x_B S_+ / (1 - y_2) |\mathcal{V}_{\text{cs}}|^2 f_Q(\eta, Q^2), \\ F_3^0(x_B, Q^2) &= |\mathcal{V}_{\text{cs}}|^2 \mathcal{B}_3 f_Q(\eta, Q^2) = 2 R_+ |\mathcal{V}_{\text{cs}}|^2 f_Q(\eta, Q^2). \end{aligned} \quad (4.17)$$

Here, we follow the notation of Ref. [28], where $R_+ = S_+/2 = g^2/16$. The coefficients \mathcal{B}_i in Eq. (4.17) are the Born coefficient functions $C_i^{(0)}$ that enter the normalization condition Eq. (4.6).

4.4 $\mathcal{O}(\alpha_s)$ coefficient functions

We did not discuss the calculation of the $\mathcal{O}(\alpha_s)$ corrections, but they are relatively straightforward to obtain following the same steps as in the higher-order calculation detailed in this paper.

The coefficients are given for the flavor-stripped tensors defined in Eq. (2.10). At this order, the only nonvanishing contributions are proportional to $|V_{\text{cs}}|^2$ (and $|V_{\text{cd}}|^2$); all other CKM structures vanish. The corresponding CKM factors are reinstated when required. The structure of the $\mathcal{O}(\alpha_s)$ contribution to the coefficient functions is

$$C_{j,n}^{(1)} = C_F \left(c_{j,n}^{(1),f} + \sum_{k=-1,1}^1 \mathcal{D}_k(y_1) c_{j,n}^{(1),k} \right). \quad (4.18)$$

where $C_{j,\bar{Q}}^{(1)} = 0$ and the $n = Q$ coefficients read

$$\begin{aligned} c_{j,Q}^{(1),1} &= -2, \\ c_{j,Q}^{(1),0} &= -\frac{7 + 4 G(0, y_2)}{2}, \\ c_{j,Q}^{(1),-1} &= S_{j,Q}^{(1)} + V_{j,Q}^{(1)} = -2 G(1, y_2) G(0, y_2) - \frac{3}{2} G(0, y_2) \\ &\quad + 2 G(0, 1, y_2) - \frac{\pi^2}{3} - \frac{5}{2} + (1 - \delta_{2j}) \frac{y_2}{1 - y_2} G(0, y_2), \end{aligned}$$

for $j = 1, 2, 3$. The first two coefficients are in fact universal for all j ; the Kronecker delta selects the term for $j \neq 2$. The remaining *finite* coefficients $c_{j,n}^{(1),f}$ take the following form

$$c_{1,Q}^{(1),f} = \frac{2G(0, y_1 y_2) A_1 - (1 - y_1 y_2) B_1}{2(1 - y_1 y_2)^3}, \quad (4.19)$$

$$c_{2,Q}^{(1),f} = \frac{2G(0, y_1 y_2) A_2 - (1 - y_1 y_2) B_2}{2(1 - y_1)(1 - y_1 y_2)^3}, \quad (4.20)$$

$$c_{3,Q}^{(1),f} = \frac{2G(0, y_1 y_2) A_3 - (1 - y_1 y_2) B_3}{2(1 - y_1 y_2)^2}, \quad (4.21)$$

with

$$\begin{aligned} A_1 &= (1 + y_1 y_2) A_3 + 2(1 - 2y_2) y_2 y_1^2 + 4y_2 (4y_2 - 1) y_1, \\ A_2 &= y_1 (y_2 - 1) A_1 + (14y_2^2 - 17y_2 + 4) y_2 y_1^3 \\ &\quad - 2(13y_2^2 - 17y_2 + 8) y_2 y_1^2 + (-2y_2^2 + 16y_2 - 1) y_1 - 8y_2 + 2, \\ A_3 &= (-2y_2^2 + 2y_2 - 1) y_2 y_1^2 + (6y_2 - 1) y_1 - 6y_2 + 2, \end{aligned}$$

and

$$\begin{aligned}
B_1 &= \left(y_1 y_2 - \frac{23}{7} \right) B_3 + \frac{2}{7} (53 y_1 - 150) - \frac{2}{7} (7 y_1^2 + 94 y_1 - 128) y_2, \\
B_2 &= \left(y_1 y_2 + \frac{24 - 11 y_1}{7} \right) B_1 + \frac{4}{7} (4 y_1^2 - 59 y_1 + 126) y_2^2 y_1 \\
&\quad - \frac{2}{7} (10 y_1^2 - 143 y_1 + 127) y_2 y_1 - \frac{2}{7} (10 y_1^2 + 9 y_1 - 71), \\
B_3 &= 9 y_2 + (7 y_2^2 - 10 y_2 + 4) y_1 - 10.
\end{aligned}$$

It is straightforward to verify that our $\mathcal{O}(\alpha_S)$ result reduces to the $\overline{\text{MS}}$ one in the limit $m^2/Q^2 \rightarrow 0$. Following Ref. [28] and using their variables that are better suited to study the high-virtuality/low-mass limit (Eq. (A.8)), we obtain in the aforementioned limit

$$\begin{aligned}
\lim_{m \rightarrow 0} \int_{\eta}^1 \frac{d\xi'}{\xi'} f_Q \left(\frac{\eta}{\xi'}, \mu_F^2 \right) C_{j,Q}^{(1)} \left(\xi', \frac{m^2}{Q^2}, \mu_R^2 \right) = \\
\int_{\eta}^1 \frac{d\xi'}{\xi'} f_Q \left(\frac{\eta}{\xi'}, \mu_F^2 \right) \left[C_{j,Q}^{\overline{\text{MS}},(1)} \left(\xi', \frac{Q^2}{\mu_F^2}, \mu_R^2 \right) + \alpha_S(\mu_R) C_{j,Q}^{\overline{\text{MS}},(0)} \Gamma_{QQ}^{(0)}(\xi', \mu_F, m) \right]. \quad (4.22)
\end{aligned}$$

We have verified that our $C_{j,Q}^{\overline{\text{MS}},(i)}$ functions are the same as, e.g., the ones presented in Ref. [42] (and references therein). The expression $\Gamma_{QQ}^{(0)}$ is nothing but the generalized quasi-collinear counter term that describes a “heavy quark inside of a heavy quark” within ACOT scheme [11, 12] and corresponds to the so-called PDF matching coefficient within the FONLL scheme [16]

$$\begin{aligned}
\Gamma_{QQ}^{(0)}(\xi', \mu_F, m) &= C_F \delta(1 - \xi') \left(2 + \frac{3}{2} \log \frac{\mu_F^2}{m^2} \right) + \\
&\quad C_F \left[\frac{1 + \xi'^2}{1 - \xi'} \left(\log \frac{\mu_F^2}{m^2(1 - \xi')^2} - 1 \right) \right]_+. \quad (4.23)
\end{aligned}$$

Unlike Ref. [28], we additionally accounted for the fermion number conservation at the leading-logarithmic level. Namely, we have verified that

$$\int_0^1 d\xi' \Gamma_{QQ}^{(0)}(\xi', \mu, m) = 0,$$

which, subsequently, ensures that we indeed reproduce the $\overline{\text{MS}}$ result in Eq. (4.22).

4.5 $\mathcal{O}(\alpha_s^2)$ coefficient functions

At this order, coefficient functions proportional to $|V_{ud}|^2$ and $|V_{us}|^2$ appear for the first time. We therefore restore the CKM matrix elements and reintegrate them into the coefficient functions, which are no longer flavor-stripped.

The complexity of the $\mathcal{O}(\alpha_s^2)$ corrections necessitates the decomposition

$$C_{j,n}^{(2)} = |V_{cd}|^2 (L_{j,n} + \theta(y_1 - 4y_2) H_{j,n}) + |V_{ud}|^2 \theta(y_1 - y_2) K_{j,n}, \quad j = 1, 2, 3, \quad (4.24)$$

where the θ functions implement the heavy-quark production thresholds at $y_1 = y_2$ and $y_1 = 4y_2$. The light term $L_{j,n}$ receives contributions from the VV, RV, and RRA cuts (see Tab. 1), the heavy term $H_{j,n}$ receives contributions solely from the RRB cut, and the remaining heavy term $K_{j,n}$ arises from the RRC cut.⁸ For the cuts contributing to $L_{j,n}$, the antiquark-initiated process vanishes identically, i.e. $L_{j,\bar{Q}} = 0$.

The color structure of the light coefficient is

$$L_{j,Q} = C_F^2 L_{1,j} + C_A C_F L_{2,j} + n_L C_F L_{3,j} + n_H C_F L_{4,j}, \quad (4.25)$$

where each color-stripped function $L_{i,j}$ ($i = 1, \dots, 4$) admits an expansion in plus-distributions analogous to the $\mathcal{O}(\alpha_s)$ case,

$$L_{i,j} = c_{i,j,L}^{(2),f} + \sum_{k=-1}^3 \mathcal{D}_k(y_1) c_{i,j,L}^{(2),k}, \quad (4.26)$$

with the distributions \mathcal{D}_k defined as before. In the following, we present only the plus-distribution coefficients $c_{i,j,L}^{(2),k}$ for $k = -1, 0, \dots, 3$ while the soft structure of H/\bar{H} is discussed later. Note that the $n_H C_F$ term, while associated with heavy-quark loops, contributes to $L_{j,Q}$ via the RV cut of diagrams with a heavy-quark loop insertion (see Fig. 3).

The plus-distribution coefficients for $k = 1, 2, 3$ read

$$\begin{aligned} c_{1,j,L}^{(2),3} &= 2, \\ c_{1,j,L}^{(2),2} &= \frac{21 + 12 G(0, y_2)}{2}, \\ c_{2,j,L}^{(2),2} &= \frac{11}{2}, \\ c_{3,j,L}^{(2),2} &= -1, \\ c_{1,j,L}^{(2),1} &= 4G(0, y_2)^2 + \left(4G(1, y_2) + \frac{15y_2 - 17}{y_2 - 1}\right)G(0, y_2) - 4G(0, 1, y_2) \\ &\quad + \frac{69}{4} + \delta_{2j} \frac{2y_2}{1 - y_2} G(0, y_2), \\ c_{2,j,L}^{(2),1} &= \frac{22}{3}G(0, y_2) - \frac{11}{3}G(1, y_2) + 2\zeta(2) + \frac{95}{36}, \\ c_{3,j,L}^{(2),1} &= -\frac{4}{3}G(0, y_2) + \frac{2}{3}G(1, y_2) - \frac{13}{18}. \end{aligned} \quad (4.27)$$

⁸The designations “light” and “heavy” distinguish contributions with light or heavy final states, respectively. Both kind of functions retain the full heavy-quark mass dependence.

For $k = 0$ the coefficients are

$$\begin{aligned}
c_{1,j,L}^{(2),0} &= (4G(1, y_2) + \frac{y_2-3}{y_2-1})G(0, y_2)^2 \\
&\quad + (7G(1, y_2) - 4G(0, 1, y_2) + \frac{41-27y_2}{4-4y_2})G(0, y_2) - 7G(0, 1, y_2) \\
&\quad - 2\zeta(3) + 3\zeta(2) + \frac{67}{8} + \delta_{2j} \frac{y_2}{1-y_2} \frac{G(0, y_2)(4G(0, y_2) + 7)}{2}, \\
c_{2,j,L}^{(2),0} &= \frac{11}{6}G(0, y_2)^2 - \frac{11}{3}G(1, y_2)G(0, y_2) + 2\zeta(2)G(0, y_2) \\
&\quad - \frac{34}{9}G(0, y_2) - \frac{77}{12}G(1, y_2) + \zeta(3) + \frac{17}{3}\zeta(2) - \frac{905}{72}, \\
c_{3,j,L}^{(2),0} &= -\frac{1}{3}G(0, y_2)^2 + \frac{2}{3}G(1, y_2)G(0, y_2) + \frac{4}{9}G(0, y_2) \\
&\quad + \frac{7}{6}G(1, y_2) - \frac{2}{3}\zeta(2) + \frac{85}{36}.
\end{aligned} \tag{4.28}$$

Here, most coefficients are independent of j with the exception: the C_F^2 contribution ($i = 1$) to $C_{2,L}^{(2)}$ contains an additional term proportional to δ_{2j} (Kronecker delta) which is similar to the previous order.

The $k = -1$ (delta-function) coefficients, together with the regular finite parts $c_{i,j,L}^{(2),f}$, are too lengthy to present here and are provided in the auxiliary material described later. The leading coefficient of the Taylor expansions of the delta-term coefficients in the $m^2/Q^2 \rightarrow 0$ limit, however, are compact

$$\begin{aligned}
c_{1,j,L}^{(2),-1} &= \left(\frac{9}{8} - 2\zeta(2)\right) \log^2\left(\frac{m^2}{Q^2}\right) + \left(-\zeta(2) - 2\zeta(3) + \frac{27}{8}\right) \log\left(\frac{m^2}{Q^2}\right) \\
&\quad + \frac{1}{8}(110\zeta(2) - 54\zeta(4) - 88\zeta(3) + 95) - 12\zeta(2)\log(2) + \mathcal{O}\left(\frac{m^2}{Q^2}\right), \\
c_{2,j,L}^{(2),-1} &= \frac{11}{8} \log^2\left(\frac{m^2}{Q^2}\right) + \left(-\frac{11}{3}\zeta(2) + 3\zeta(3) - \frac{35}{8}\right) \log\left(\frac{m^2}{Q^2}\right) \\
&\quad + \frac{1}{72}(-1610\zeta(2) + 819\zeta(4) + 804\zeta(3) - 1081) \\
&\quad + 6\zeta(2)\log(2) + \mathcal{O}\left(\frac{m^2}{Q^2}\right), \\
c_{3,j,L}^{(2),-1} &= -\frac{1}{4} \log^2\left(\frac{m^2}{Q^2}\right) + \left(\frac{2}{3}\zeta(2) + \frac{3}{4}\right) \log\left(\frac{m^2}{Q^2}\right) \\
&\quad + \frac{1}{36}(82\zeta(2) - 24\zeta(3) + 71) + \mathcal{O}\left(\frac{m^2}{Q^2}\right), \\
c_{4,j,L}^{(2),-1} &= \frac{1}{9} \log^3\left(\frac{m^2}{Q^2}\right) + \frac{19}{18} \log^2\left(\frac{m^2}{Q^2}\right) + \left(\frac{2}{3}\zeta(2) + \frac{265}{54}\right) \log\left(\frac{m^2}{Q^2}\right) \\
&\quad + \frac{5}{9}\zeta(2) - \frac{2}{3}\zeta(3) + \frac{7951}{648} + \mathcal{O}\left(\frac{m^2}{Q^2}\right),
\end{aligned} \tag{4.29}$$

where we have again used the variable change from Eq. (A.8). We emphasize the term $c_{4,j,L}^{(2),-1}$, proportional to $n_H C_F$, diverges as $\log^3\left(\frac{m^2}{Q^2}\right)$ as the ratio grows, as anticipated

in Sec. 4.2. The soft-divergent diagrams were shown prior in Fig. 3. The coefficient $L_{4,j}$ contributes only to the $k = -1$ (delta function) term and all its plus-distribution as well as finite coefficients vanish: $c_{4,j,L}^{(2),-1} = 0$ for $k \geq 0$.

The heavy coefficients admit the following color decomposition

$$H_{j,Q} = C_F \left(C_F - \frac{C_A}{2} \right) H_{1,j} + C_F (H_{2,j} + n_H H_{3,j}), \quad (4.30)$$

$$H_{j,\bar{Q}} = C_F \left(C_F - \frac{C_A}{2} \right) \bar{H}_{1,j} + C_F (\bar{H}_{2,j} + n_H \bar{H}_{3,j}). \quad (4.31)$$

Here, the sea contributions are the same, $H_{2,j} = \bar{H}_{2,j}$. As discussed in Sec. 4.2, for $m \neq 0$, the heavy coefficient functions $H/\bar{H}_{i,j}(\xi', m)$ themselves are finite (non-singular) for all ξ' in the physical region. Therefore, they do not require a plus-prescription regularization to be integrated.

However, the soft divergence emerges in the $m^2/Q^2 \rightarrow 0$ limit. The resulting large triple logarithm is generated solely by the term proportional to $n_H C_F$. To isolate this singular behavior, we consider the asymptotic expansion of $H_{j,n}$ as $m \rightarrow 0$. The correct asymptotic form is obtained by applying a combination of Taylor and asymptotic expansion operators, T and A , defined as in Eq. (4.10). Letting T_{m^2} and $A_{\xi'}$ denote expansion in m^2/Q^2 and asymptotic expansion in ξ' , respectively, we have

$$\begin{aligned} \lim_{m \rightarrow 0} \int_{\eta}^{\xi'_{\text{th}}} \frac{d\xi'}{\xi'} f_Q \left(\frac{\eta}{\xi'} \right) H_{3,j}(\xi', m) \rightarrow \\ \int_{\eta}^1 \frac{d\xi'}{\xi'} f_Q \left(\frac{\eta}{\xi'} \right) \left(H_{3,j}^{(0)} - T_{\xi'} \circ T_{m^2} [H_{3,j}] + A_{\xi'} T_{m^2} \circ [H_{3,j}] \right) + \mathcal{O} \left(\frac{m^2}{Q^2} \right). \end{aligned} \quad (4.32)$$

The term $T_{m^2} \circ T_{\xi'} [H_{3,j}]$ subtracts the Taylor expansion of $H_{3,j}$ around $\xi' = 0$, which contains an artifact behaving as $1/(1 - \xi')$ that is not singular at finite mass but would otherwise pollute the asymptotic extraction. The structure of the heavy coefficients reads

$$A_{\xi'} T_{m^2} \circ [H_{3,j}] = \sum_{k=-1}^2 \mathcal{D}_k(y_1) c_{j,H}^{(2),k}, \quad \text{where} \quad (4.33)$$

$$c_{j,H}^{(2),2} = \frac{1}{3}, \quad (4.34)$$

$$c_{j,H}^{(2),1} = -\frac{2}{3} \log \left(\frac{m^2}{Q^2} \right) - \frac{29}{18}, \quad (4.35)$$

$$c_{j,H}^{(2),0} = \frac{1}{3} \log^2 \left(\frac{m^2}{Q^2} \right) + \frac{29}{18} \log \left(\frac{m^2}{Q^2} \right) - \frac{2\zeta(2)}{3} + \frac{359}{108}, \quad (4.36)$$

$$\begin{aligned} c_{j,H}^{(2),-1} = & -\frac{1}{9} \log^3 \left(\frac{m^2}{Q^2} \right) - \frac{29}{36} \log^2 \left(\frac{m^2}{Q^2} \right) \\ & + \left(\frac{2\zeta(2)}{3} - \frac{359}{108} \right) \log \left(\frac{m^2}{Q^2} \right) \\ & - \frac{8 \log^3(2)}{9} + \frac{29 \log^2(2)}{9} + \left(\frac{4\zeta(2)}{3} - \frac{359}{54} \right) \log(2). \end{aligned} \quad (4.37)$$

Thus, for $s > 4m^2$, combining the $n_H C_F$ terms from the light and heavy contributions (Eqs. (4.29, 4.33), respectively), we obtain

$$L_{4,j} + H_{3,j} \longrightarrow n_H C_F \mathcal{D}_{-1}(\xi') \left(c_{4,j,L}^{(2),-1} + c_{j,H}^{(2),-1} \right) + \dots \approx \mathcal{O} \left(\log^2 \left(\frac{m^2}{Q^2} \right) \right), \quad (4.38)$$

so that the potentially large triple logarithm cancels exactly, in analogy with Refs. [18, 19]. The inclusion of diagrams (specifically VV and RV cuts in Fig. 3) contributing to these large logarithms in the region $s < 4m^2$ is subject to the exact definition of the corresponding hadron function as discussed in Ref. [16]. Our default calculation includes these diagrams. A variant excluding their contribution, along with the relevant auxiliary files, can be provided upon request.

The color structure of the contributions proportional to $|V_{ud}|^2$ (and $|V_{us}|^2$) is straightforward, as it is entirely proportional to C_F . Apart from this, the functions $K_{j,n}$ do not exhibit any additional structure relevant for the present discussion; they are expressible in terms of Goncharov polylogarithms with rational prefactors.

The remaining finite contributions, such as $c_{i,j,L}^{(2),f}$ and their heavy counterparts, are too extensive to be listed here. They are provided in full, together with the singular coefficients presented above, in an auxiliary file whose structure is described in the following section.

4.6 Auxiliary files and validation

The analytic expressions for the coefficient functions presented in this publication can be obtained by cloning the repository from the system command line

```
git clone https://github.com/Qdashkin/CF_HQI_CC_DIS.git
```

or by downloading the source directly from the GitHub webpage using the URL above. The repository contains three main files:

- **README.md**: a standard **README** file with a description of the repository.
- **strFun.nb**: a **Mathematica** notebook containing the analytic results and documentation.
- **strFun.mx**: a **Mathematica** storage file containing the notebook's pre-evaluated definitions for direct loading.

The notebook **strFun.nb** includes:

- The coefficient functions at leading order (Eq. (4.17)).
- The $\mathcal{O}(\alpha_s)$ coefficient functions (Eq. (4.18)).
- The $\mathcal{O}(\alpha_s^2)$ coefficient functions (Eq. (4.24)), with the light ($L_{j,n}$) and heavy ($H_{j,n}$ and $K_{j,n}$) terms provided separately.
- The correct heavy-flavor soft term (Eq. (4.32)).

It also documents all definitions and explicitly notes the (few) instances where the notation departs from that used in the preceding sections.

We discuss now the validation of our results through a series of independent checks starting with the leading order: our Born results agree exactly with those of Ref. [11], providing a first consistency test.

At $\mathcal{O}(\alpha_s)$, we have verified our expressions against Ref. [28] by expanding their general result in the limit $m_2 \rightarrow 0$ and using the prescription of Ref. [82] to correctly reconstruct the finite term.⁹ Furthermore, by expanding our coefficient functions in the $m \rightarrow 0$ limit and incorporating the generalized counter-term from Eq. (4.23), we have explicitly reproduced the well-known $\mathcal{O}(\alpha_s)$ $\overline{\text{MS}}$ DIS results from Ref. [83] in Eq. (4.22).

The most robust check of the $\mathcal{O}(\alpha_s^2)$ corrections presented in this work is their asymptotic expansion. For the heavy-quark initiated partonic structure functions, it reads

$$C_{0,j,n}^{(2)} = \tilde{C}_{0,j,n}^{(2),0} + y_2^{-\epsilon} \tilde{C}_{0,j,n}^{(2),1} + y_2^{-2\epsilon} \tilde{C}_{0,j,n}^{(2),2} + \mathcal{O}(y_2), \quad (4.39)$$

where the leading coefficient $\tilde{C}_{0,j,n}^{(2),0}$ is the unrenormalized (bare) contribution in the massless-limit. We have verified analytically that this coefficient coincides exactly with the unrenormalized partonic structure functions appearing in the purely massless calculations. The agreement is not accidental: it is a consequence of the decoupling theorem [84] and its refined analysis given in Ref. [85] within the dimensional regularization that makes this decoupling manifest at the level of scattering amplitudes for finite ϵ .

To obtain the bare massless coefficient functions of Ref. [42], we independently recomputed their $\overline{\text{MS}}$ result using the same approach as in the current work, thereby obtaining direct access to the bare functions. This independent calculation provides an additional, robust verification of our computational framework. Furthermore, expanding Eq. (4.39) in the $\epsilon \rightarrow 0$ limit reproduces the Taylor expansion of our exact (mass-dependent) bare coefficient functions $C_{0,j,n}^{(2)}$. This consistency, together with the numerical check of the master integrals via **AMFlow** [70] as discussed in Sec. 3.5, further ensures the correctness of our results.

We have also computed the bare virtual function, which was not discussed explicitly in the main text. In attempting to verify its ϵ -pole structure against the results of Refs. [86, 87], we were able to match the $\mathcal{O}(\epsilon^{-2})$ poles, but found a discrepancy in the $\mathcal{O}(\epsilon^{-1})$ and finite terms. This mismatch could arise from an incorrect application of the formulas in those references to our specific kinematics, or it may reflect a genuine difference: the diagrams in the cited works do not cover the case of a gluon connecting a massive and a massless quark line at the vertex (Fig. 3). Regardless of this partial cross-check, we note that within our calculation the poles from the virtual and soft contributions cancel, and the fully renormalized result is finite. This internal consistency provides strong support for the correctness of our virtual function and, by extension, the full renormalized coefficient functions.

We note that the $\overline{\text{MS}}$ coefficient functions at $\mathcal{O}(\alpha_s^2)$ could, in principle, also be extracted by a procedure analogous to that described in Sec. 4.4. This would, however, require

⁹Ref. [28] considers the most general two-flavor case at $\mathcal{O}(\alpha_s)$, which includes an extra mass parameter m_2 .

counter-terms analogous to Eq. (4.23) at one higher order, which are not yet available but can be computed using methods such as those in Refs. [18, 88]. In a forthcoming publication [41], we will instead extract these very counter-terms from the present calculation itself. Indeed, the remaining coefficients $\tilde{C}_{0,j,n}^{(2),1}$ and $\tilde{C}_{0,j,n}^{(2),2}$ correspond to operator matrix elements entering the operator product expansion discussed in, for instance, Ref. [19].

5 Summary and outlook

We have presented the computational details of the charged-current deep-inelastic scattering coefficient functions through $\mathcal{O}(\alpha_s^2)$, retaining full heavy-quark mass dependence. Modern variable-flavor number schemes such as ACOT and FONLL require $n_L = 3$ active flavors as the initial condition in the evolution equations; accordingly, we used the decoupling scheme to renormalize the UV divergences, keeping only n_L active flavors. We provided a detailed discussion of the structure of the coefficient functions and isolated the soft singularities, thereby enabling the subsequent convolution with PDFs. The results are provided as a supplementary **Mathematica** notebook file on GitHub.

Although the existence of intrinsic heavy flavor, such as charm, remains an open question, our result provides one of the last essential contributions to inclusive DIS at NNLO and will facilitate its determination. In a more conservative scenario, our calculation is indispensable for quantifying the underlying theoretical uncertainties in current PDF fits or in the future N³LO.

We expect that, once the remaining PDF matching coefficients, which are a direct outcome of this work, become available [41], a thorough phenomenological analysis including the presented results of charged-current DIS will be possible. In particular, it will be interesting to probe CC DIS near threshold and at high values of virtuality, where the effects of the heavy quark are numerically significant. This will clarify the impact of heavy flavors on predictions relevant for future experiments such as FASER at the LHC, complementing the study in Ref. [14].

Acknowledgments

We are indebted to Stefano Forte and Felix Hekhorn for their interest and substantial support throughout this work. We are grateful to Roman N. Lee for assistance with his package **Libra** [60]. We thank Marco Bonetti and Hai Tao Li for a careful reading of the manuscript and various conversations about the project. We also thank the following for helpful discussions: Konstantin Asteriadis, Arnd Behring, Daniel Baranowski, Long Chen, Maximilian Delto, Zhe Li and Jian Wang. This work is supported by the National Science Foundation of China under grants No. 12275156 and No. 12321005. Additionally, this work was started at the physics department of Milan University and partly supported by the European Research Council under the European Union’s Horizon 2020 research and innovation Programme (grant agreement n.740006).

A Auxiliaries

A.1 Parton kinematics

Following Ref. [11], the standard DIS invariant variables are

$$P^2 = M^2, \quad Q^2 = -q^2, \quad x_B = \frac{Q^2}{2P \cdot q}, \quad (\text{A.1})$$

where P is the momentum of the nucleon target, q is the momentum transfer from the lepton vertex and x_B is the Bjorken variable.

Using light-cone coordinates (cf. Ref. [89]), we parameterize the momenta of the off-shell boson and incident heavy quark in the DIS collinear frame as

$$\begin{aligned} q^\mu &\equiv (q_1^+, q_1^-; \vec{q}_1^\perp) = \left(-\eta P^+, \frac{Q^2}{2\eta P^+}; \vec{0} \right), \\ p^\mu &= \left(\xi P^+, \frac{m^2}{2\xi P^+}; \vec{0} \right), \end{aligned} \quad (\text{A.2})$$

respectively. Within this parameterization, the Bjorken variable generalizes to

$$\frac{1}{\eta} = \frac{1}{2x_B} + \sqrt{\frac{1}{4x_B^2} + \frac{M^2}{Q^2}}, \quad (\text{A.3})$$

where η includes finite target-mass corrections.

The partonic center-of-mass energy relates to the momentum fraction ξ through

$$s = (q + p)^2 = \left(Q^2 + \frac{\eta}{\xi} m^2 \right) \left(\frac{\xi}{\eta} - 1 \right). \quad (\text{A.4})$$

Inverting this equation results in

$$\xi = \eta \frac{Q^2 - m^2 + s + \Delta[-Q^2, m^2, s]}{2Q^2}, \quad (\text{A.5})$$

where the triangle function is defined as usual:

$$\Delta[a, b, c] = \sqrt{a^2 + b^2 + c^2 - 2(ab + ac + bc)}. \quad (\text{A.6})$$

Using Eq. (A.5), we obtain the lower bound of the integration domain

$$\xi_{\text{th}} = \begin{cases} \eta, & (s = 0) \\ \eta \frac{1 + \sqrt{1 + 4m^2/Q^2}}{2}, & (s = m^2) \\ \eta \frac{Q^2 + 3m^2 + \Delta[-Q^2, m^2, 4m^2]}{2Q^2}, & (s = 4m^2) \end{cases} \quad (\text{A.7})$$

corresponding to the virtual and heavy-quark pair production thresholds, respectively. The upper bound follows from momentum conservation, giving the integration domain $\xi_{\text{th}} \leq \xi \leq 1$ in Eq. (2.3).

In Ref. [28], a different scaling variable is introduced. Its definition reads

$$\xi' = \frac{\eta}{\xi}. \quad (\text{A.8})$$

This one is related to our choice of variables in Eq. (3.12) via

$$y_1 \rightarrow 1 - \xi', \quad y_2 = m^2 \frac{\xi'}{Q^2 + m^2 \xi'}. \quad (\text{A.9})$$

A.2 Projectors, normalization and γ_5 schemes

We work in dimensional regularization with $d = 4 - 2\epsilon$, using standard Clifford algebra relations. Special care is required when evaluating traces involving γ_5 , which appears in the charged weak current defined in Eq. (2.8).

The complication arises because γ_5 is intrinsically four-dimensional and cannot be consistently continued to d dimensions: one cannot simultaneously preserve its anticommutation relation $\{\gamma_\mu, \gamma_5\} = 0$ and the cyclicity of traces involving γ_5 in d dimensions [90, 91].

Several schemes address this by compromising different algebraic properties. The Breitenlohner–Maison–t’ Hooft–Veltman (HVBM) scheme [92–94] provides a consistent framework by abandoning the anticommutation relation $\{\gamma_\mu, \gamma_5\} = 0$ for $\mu > 4$. In contrast, Kreimer’s approach [91, 95] aims to preserve the cyclicity of traces but is less widely adopted in the community.

We employ two schemes to cross-check our results: Kreimer’s and Larin’s (a simplified HVBM variant) [96–98]. We refer to the original literature for technical details and summarize only the essential projectors, normalization factors, and finite renormalizations relevant to our calculation.

Traces with γ_5 introduce Levi–Civita tensors. Their contraction gives

$$\varepsilon^{\mu_1\mu_2\mu_3\mu_4}\varepsilon_{\nu_1\nu_2\nu_3\nu_4} = \det \begin{pmatrix} \delta_{\nu_1}^{\mu_1} & \cdots & \delta_{\nu_4}^{\mu_1} \\ \vdots & \ddots & \vdots \\ \delta_{\nu_1}^{\mu_4} & \cdots & \delta_{\nu_4}^{\mu_4} \end{pmatrix}, \quad (\text{A.10})$$

where $\delta_{\nu_j}^{\mu_i}$ are Kronecker deltas, with reference dimension $d = 4$ (Kreimer) or $d = 4 - 2\epsilon$ (Larin).

The projectors derived from Eqs. (2.11, 2.12) are

$$\begin{aligned} \mathcal{P}_1^{\mu\nu} &= \frac{1}{(2-d)} \left(\eta^{\mu\nu} + \frac{1}{\Delta'} \left\{ -Q^2 p_1^\mu p_1^\nu + m^2 p_2^\mu p_2^\nu + (Q^2 - m^2 + s)(p_1^\mu p_2^\nu + p_2^\mu p_1^\nu) \right\} \right), \\ \mathcal{P}_2^{\mu\nu} &= \frac{4}{(d-2)\Delta'} \left\{ -Q^2 \eta^{\mu\nu} + \frac{2}{\Delta'} \left[2(d-1)(Q^2)^2 p_2^\mu p_2^\nu \right. \right. \\ &\quad + \left(\frac{1}{2}(d-2)(Q^2 - m^2 + s)^2 - 2m^2 Q^2 \right) p_1^\mu p_1^\nu \\ &\quad \left. \left. + (d-1)Q^2 (Q^2 - m^2 + s)(p_1^\nu p_2^\mu + p_1^\mu p_2^\nu) \right] \right\}, \\ \mathcal{P}_3^{\mu\nu} &= -\frac{4i}{\Delta'} \varepsilon^{\mu\nu\alpha\beta} p_{1,\beta} p_{2,\alpha}, \end{aligned} \quad (\text{A.11})$$

where the Levi–Civita tensor is taken to be strictly four-dimensional to derive the corresponding projectors and $\Delta' = \Delta[-Q^2, m^2, s]$. These projectors are directly applicable in Kreimer’s scheme but require modifications for Larin’s scheme.

Kreimer’s scheme is implemented straightforwardly following Ref. [95]. The main technical complication arises from scalar products of the form $\bar{\eta}_{\mu\nu} l_1^\mu l_2^\nu$, where the four-dimensional Minkowski tensor $\bar{\eta}_{\mu\nu}$ originates from contractions of pairs of LC tensors.

These can be evaluated either:

- by Passarino-Veltman reduction [99], which expresses $l_1^\mu l_2^\nu$ in terms of scalars and external tensors before contracting with $\bar{\eta}_{\mu\nu}$; or
- via generating functions from Symanzik polynomials as detailed in Refs [100, 101], where -2ϵ -dimensional scalar products are replaced with combinations of inverse propagators.

We used the first method for all such scalar products. Where applicable, the second method provided a valuable cross-check of the results obtained with the first.

We implement Larin's scheme following Ref. [102]. Spurious coefficients from products of Levi-Civita tensors in d dimensions are corrected via

$$\begin{aligned} F_1 : A^2 &\rightarrow \frac{6}{(d-2)(d-3)(d-7)} A^2, \\ F_2 : A^2 &\rightarrow -\frac{2}{(d-2)(d-3)} A^2, \\ F_3 : VA &\rightarrow \frac{1}{(d-2)(d-3)} VA, \end{aligned} \tag{A.12}$$

where V and A denote vector and axial parts of the vertex (cf. Eq. (2.8)).

To restore the axial Ward identity, we apply finite renormalization to the axial current $A \rightarrow Z_A Z_5 A$ [96]

$$\begin{aligned} Z_A &= 1 + \frac{C_F}{2\epsilon} \left(\frac{\alpha_s}{2\pi} \right)^2 \left(\frac{11C_A - 6n_f}{3} \right) + \mathcal{O}(\alpha_s^3), \\ Z_5 &= 1 - 2C_F \left(\frac{\alpha_s}{2\pi} \right) \\ &\quad + \left(\frac{\alpha_s}{2\pi} \right)^2 \left(\frac{11}{2} C_F^2 - \frac{107}{36} C_F C_A + \frac{1}{18} C_F n_f \right) + \mathcal{O}(\alpha_s^3). \end{aligned} \tag{A.13}$$

B Master integrals material

Alphabets. The relevant alphabets appearing in Eq. (3.14) are listed below. The remaining alphabets from that equation are not used and are therefore omitted.

$$\{a_{2,i}^I\} = \left\{ 0, -1, -\frac{1}{2}, 1 - y_1, \frac{1}{2}(1 - y_1), -\frac{y_1}{4}, -\frac{1}{y_1}, \frac{1}{y_1}, \frac{1}{y_1 - 4}, \frac{1}{y_1 - 3}, \frac{1 - y_1}{y_1}, -\frac{y_1}{y_1 + 1}, -\frac{y_1}{y_1 + 2} \right\}, \tag{B.1}$$

$$\{a_{2,i}^Q\} = \left\{ 0, \frac{1 - y_1}{y_1} \right\}, \tag{B.2}$$

$$\{a_{2,i}^{II}\} = \left\{ 0, 1, 2 - y_1, \frac{1}{y_1}, y_1, \frac{y_1}{2y_1 - 1} \right\}, \tag{B.3}$$

$$\{a_{1,i}^{III}\} = \left\{ 0, -1, -\frac{1}{y_2}, \frac{1}{y_2}, \frac{1 - y_2}{y_2}, \frac{1}{y_2 - 1}, \frac{2}{y_2 - 1}, \frac{1}{2y_2 - 1} \right\},. \tag{B.4}$$

The alphabets listed below appear in the systems for boundary conditions as in Eq.(3.20).

$$\{b_i^I\} = \{0, 1, 2\}, \quad (B.5)$$

$$\{b_i^{II}\} = \{0, 1, 2\}, \quad (B.6)$$

$$\{b_i^{III}\} = \{0, 1\}, \quad (B.7)$$

$$\{b_i^{IV}\} = \{0, 1, -1, 1/2\}, \quad (B.8)$$

$$\begin{aligned} \{a^u\} = & \left\{ 0, -1, -2, -\frac{2}{2-y_1}, -\frac{2(1-y_1)}{2-y_1}, \frac{y_1}{r_1} - 1, -\frac{y_1}{r_1} - 1, \frac{y_1}{r_2} - 1, \right. \\ & -\frac{y_1}{r_2} - 1, \frac{y_1}{r_3} - 1, -\frac{y_1}{r_3} - 1, \frac{r_3 + y_1 - 2}{2-y_1}, \frac{r_3 - y_1 + 2}{y_1 - 2}, \frac{y_1}{r_4} - 1, \\ & -\frac{y_1}{r_4} - 1, r_5 - 1, -r_5 - 1, r_6 - 1, -r_6 - 1, \frac{y_1}{r_7} - 1, -\frac{y_1}{r_7} - 1, \\ & \left. \frac{y_1}{r_8} - 1, -\frac{y_1}{r_8} - 1, r_9 - 1, -r_9 - 1 \right\}. \end{aligned} \quad (B.9)$$

The simplifications in the integrand (Eq. (3.22)) produce multiple square roots due to the transformation defined in Eq. (3.24) as can be seen in the sets above. We collect these below

$$\begin{aligned} r_1 &= \sqrt{(2-y_1)y_1}, \quad r_2 = \sqrt{(4-3y_1)y_1}, \quad r_3 = \sqrt{(y_1-4)y_1}, \\ r_4 &= \sqrt{(y_1-2)y_1}, \quad r_5 = \sqrt{\frac{y_1+1}{y_1-3}}, \quad r_6 = \sqrt{\frac{y_1+2}{y_1-2}}, \\ r_7 &= \sqrt{y_1-4}, \quad r_8 = \sqrt{y_1+4}, \quad r_9 = \sqrt{\frac{(y_1-3)y_1}{y_1^2-3y_1+4}}. \end{aligned} \quad (B.10)$$

Here, when working with the square roots, it is important to keep in mind the Feynman prescription which can be easily inferred via $s \rightarrow s + i0$.

Cut mappings. To obtain the cut integral families, we use the rules provided in Tab. 3. The rules are specific to our setup; for instance, families ‘fam2’ and ‘fam3’ contain multiple cuts of the same type (e.g., II'). The cut families listed above are not all independent, i.e. some can be mapped onto others, resulting in a smaller set of unique families. In our practical computation, only the cut rules for ‘fam1’ are used directly.

Cut	fam1	fam2	fam3	fam4	fam5	fam6
I'	{1, 3, 7}	—	—	{2, 3, 5}	{2, 3, 5}	—
II'	—	—	—	—	—	{1, 3, 5}
III'	{2, 4, 6}	{1, 4, 6}	{1, 4, 6}	—	—	—
IV'	{6, 7}	{3, 4}	{3, 4}	—	—	—

Table 3: On-shell propagator assignments for each cut and generic integral family. The entries list the indices i of the inverse propagators D_i (defined in Tab. 2) to be put on-shell according to Eq. (3.3).

Normalization. The factors f_i are

$$\begin{aligned} f_{\text{I}} &= \frac{(16\pi^2)^2}{2\pi} \cdot (2 - 13\epsilon + 27\epsilon^2 - 18\epsilon^3), \\ f_{\text{II}} &= \frac{(16\pi^2)^2}{\pi} \cdot \epsilon \frac{-2 + 13\epsilon - 27\epsilon^2 + 18\epsilon^3}{2(\epsilon - 1)}, \\ f_{\text{III}} &= 2 \frac{(16\pi^2)^2}{\pi} \cdot \epsilon(1 - 3\epsilon + 2\epsilon^2), \\ f_{\text{IV}} &= 2 \frac{(16\pi^2)^2}{2} \cdot \epsilon^2(2 - 7\epsilon + 6\epsilon^2). \end{aligned} \quad (\text{B.11})$$

The overall factor of 2 in f_{III} and f_{IV} originates from the optical theorem (Eq. (2.16)); remaining prefactors are chosen to obtain the UT form of master integral and for general convenience.

References

- [1] E. Witten, *Heavy Quark Contributions to Deep Inelastic Scattering*, *Nucl. Phys. B* **104** (1976) 445.
- [2] S.J. Brodsky, P. Hoyer, C. Peterson and N. Sakai, *The Intrinsic Charm of the Proton*, *Phys. Lett. B* **93** (1980) 451.
- [3] J. Blümlein, *A Kinematic Condition on Intrinsic Charm*, *Phys. Lett. B* **753** (2016) 619 [[1511.00229](#)].
- [4] T.-J. Hou et al., *New CTEQ global analysis of quantum chromodynamics with high-precision data from the LHC*, *Phys. Rev. D* **103** (2021) 014013 [[1912.10053](#)].
- [5] A. Ablat et al., *New results in the CTEQ-TEA global analysis of parton distributions in the nucleon*, *Eur. Phys. J. Plus* **139** (2024) 1063 [[2408.04020](#)].
- [6] L.A. Harland-Lang, A.D. Martin, P. Motylinski and R.S. Thorne, *Parton distributions in the LHC era: MMHT 2014 PDFs*, *Eur. Phys. J. C* **75** (2015) 204 [[1412.3989](#)].
- [7] S. Bailey, T. Cridge, L.A. Harland-Lang, A.D. Martin and R.S. Thorne, *Parton distributions from LHC, HERA, Tevatron and fixed target data: MSHT20 PDFs*, *Eur. Phys. J. C* **81** (2021) 341 [[2012.04684](#)].
- [8] NNPDF collaboration, *Parton distributions from high-precision collider data*, *Eur. Phys. J. C* **77** (2017) 663 [[1706.00428](#)].
- [9] NNPDF collaboration, *An open-source machine learning framework for global analyses of parton distributions*, *Eur. Phys. J. C* **81** (2021) 958 [[2109.02671](#)].
- [10] PDF4LHC WORKING GROUP collaboration, *The PDF4LHC21 combination of global PDF fits for the LHC Run III*, *J. Phys. G* **49** (2022) 080501 [[2203.05506](#)].
- [11] M.A.G. Aivazis, F.I. Olness and W.-K. Tung, *Leptoproduction of heavy quarks. 1. General formalism and kinematics of charged current and neutral current production processes*, *Phys. Rev. D* **50** (1994) 3085 [[hep-ph/9312318](#)].
- [12] M.A.G. Aivazis, J.C. Collins, F.I. Olness and W.-K. Tung, *Leptoproduction of heavy quarks. 2. A Unified QCD formulation of charged and neutral current processes from fixed target to collider energies*, *Physical Review D: Particles and Fields* **50** (1994) 3102 [[hep-ph/9312319](#)].

- [13] T. Stavreva, F.I. Olness, I. Schienbein, T. Jezo, A. Kusina, K. Kovarik et al., *Heavy Quark Production in the ACOT Scheme at NNLO and N3LO*, *Phys. Rev. D* **85** (2012) 114014 [[1203.0282](#)].
- [14] P. Risse, V. Bertone, T. Ježo, K. Kovařík, A. Kusina, F. Olness et al., *Heavy quark mass effects in charged-current deep-inelastic scattering at approximate NNLO in the Avazis-Collins-Olness-Tung scheme*, *Phys. Rev. D* **112** (2025) 114004 [[2504.13317](#)].
- [15] M. Cacciari, M. Greco and P. Nason, *The p_T spectrum in heavy-flavour hadroproduction.*, *JHEP* **05** (1998) 007 [[hep-ph/9803400](#)].
- [16] S. Forte, E. Laenen, P. Nason and J. Rojo, *Heavy quarks in deep-inelastic scattering*, *Nucl. Phys. B* **834** (2010) 116 [[1001.2312](#)].
- [17] R.D. Ball, M. Bonvini and L. Rottoli, *Charm in Deep-Inelastic Scattering*, *JHEP* **11** (2015) 122 [[1510.02491](#)].
- [18] I. Bierenbaum, J. Blümlein and S. Klein, *Two-Loop Massive Operator Matrix Elements and Unpolarized Heavy Flavor Production at Asymptotic Values $Q^2 \gg m^2$* , *Nucl. Phys. B* **780** (2007) 40 [[hep-ph/0703285](#)].
- [19] M. Buza, Y. Matiounine, J. Smith, R. Migneron and W.L. van Neerven, *Heavy quark coefficient functions at asymptotic values $Q^2 \gg m^2$* , *Nucl. Phys. B* **472** (1996) 611 [[hep-ph/9601302](#)].
- [20] J. Ablinger, J. Blümlein, A. De Freitas, A. Goedelke, M. Saragnese, C. Schneider et al., *The two-mass contribution to the three-loop polarized gluonic operator matrix element $A_{gg,Q}^{(3)}$* , *Nucl. Phys. B* **955** (2020) 115059 [[2004.08916](#)].
- [21] A. Behring, J. Blümlein, A. De Freitas, A. von Manteuffel, K. Schönwald and C. Schneider, *The polarized transition matrix element $A_{gg}(N)$ of the variable flavor number scheme at $O(\alpha_s^3)$* , *Nucl. Phys. B* **964** (2021) 115331 [[2101.05733](#)].
- [22] J. Ablinger, A. Behring, J. Blümlein, A. De Freitas, A. Goedelke, A. von Manteuffel et al., *The unpolarized and polarized single-mass three-loop heavy flavor operator matrix elements $A_{gg,Q}$ and $\Delta A_{gg,Q}$* , *JHEP* **12** (2022) 134 [[2211.05462](#)].
- [23] J. Ablinger, A. Behring, J. Blümlein, A. De Freitas, A. von Manteuffel, C. Schneider et al., *The first-order factorizable contributions to the three-loop massive operator matrix elements $AQg(3)$ and $\Delta AQg(3)$* , *Nucl. Phys. B* **999** (2024) 116427 [[2311.00644](#)].
- [24] J. Ablinger, A. Behring, J. Blümlein, A. De Freitas, A. von Manteuffel, C. Schneider et al., *The non-first-order-factorizable contributions to the three-loop single-mass operator matrix elements $AQg(3)$ and $\Delta AQg(3)$* , *Phys. Lett. B* **854** (2024) 138713 [[2403.00513](#)].
- [25] J. Ablinger, A. Behring, J. Blümlein, A. De Freitas, A. von Manteuffel, C. Schneider et al., *The Single-Mass Variable Flavor Number Scheme at Three-Loop Order*, [2510.02175](#).
- [26] J. Ablinger, J. Blümlein, A. De Freitas, A. von Manteuffel, C. Schneider and K. Schönwald, *The two-mass contributions to the three-loop massive operator matrix elements $\tilde{A}_{Qg}^{(3)}$ and $\Delta \tilde{A}_{Qg}^{(3)}$* , [2510.09403](#).
- [27] A. Behring, J. Blümlein, A. De Freitas, A. von Manteuffel, C. Schneider and K. Schönwald, *The heavy quark-antiquark asymmetry in the variable flavor number scheme*, [2512.13508](#).
- [28] S. Kretzer and I. Schienbein, *Heavy quark initiated contributions to deep inelastic structure functions*, *Phys. Rev. D* **58** (1998) 094035 [[hep-ph/9805233](#)].

[29] E. Spezzano, T. Jezo, M. Klasen, P. Risse and I. Schienbein, *NLO heavy-quark contributions to DIS structure functions in the ACOT scheme*, [2511.02407](https://arxiv.org/abs/2511.02407).

[30] E. Spezzano, T. Jezo, M. Klasen, P. Risse and I. Schienbein, *Heavy-quark contributions to the DIS structure functions F_4 and F_5 at NLO in the ACOT scheme*, [2512.11569](https://arxiv.org/abs/2512.11569).

[31] J. Pumplin, H.L. Lai and W.K. Tung, *The Charm Parton Content of the Nucleon*, *Phys. Rev. D* **75** (2007) 054029 [[hep-ph/0701220](https://arxiv.org/abs/hep-ph/0701220)].

[32] NNPDF collaboration, *Evidence for intrinsic charm quarks in the proton*, *Nature* **608** (2022) 483 [[2208.08372](https://arxiv.org/abs/2208.08372)].

[33] FASER collaboration, *First Direct Observation of Collider Neutrinos with FASER at the LHC*, *Phys. Rev. Lett.* **131** (2023) 031801 [[2303.14185](https://arxiv.org/abs/2303.14185)].

[34] SND@LHC collaboration, *Observation of Collider Muon Neutrinos with the SND@LHC Experiment*, *Phys. Rev. Lett.* **131** (2023) 031802 [[2305.09383](https://arxiv.org/abs/2305.09383)].

[35] J.M. Cruz-Martinez, M. Fieg, T. Giani, P. Krack, T. Mäkelä, T.R. Rabemananjara et al., *The LHC as a Neutrino-Ion Collider*, *Eur. Phys. J. C* **84** (2024) 369 [[2309.09581](https://arxiv.org/abs/2309.09581)].

[36] L.P. Das, D. Garg, M.V. Garzelli, M.H. Reno and G. Sigl, *Prompt atmospheric leptons and the potential role of intrinsic charm*, *PoS ICRC2025* (2025) 1021 [[2508.06473](https://arxiv.org/abs/2508.06473)].

[37] ICECUBE collaboration, *Evidence for High-Energy Extraterrestrial Neutrinos at the IceCube Detector*, *Science* **342** (2013) 1242856 [[1311.5238](https://arxiv.org/abs/1311.5238)].

[38] T. Cridge et al., *Combination of aN^3LO PDFs and implications for Higgs production cross-sections at the LHC*, *J. Phys. G* **52** (2025) 6 [[2411.05373](https://arxiv.org/abs/2411.05373)].

[39] NNPDF collaboration, *The path to N^3LO parton distributions*, *Eur. Phys. J. C* **84** (2024) 659 [[2402.18635](https://arxiv.org/abs/2402.18635)].

[40] J.C. Collins, *Hard scattering factorization with heavy quarks: A General treatment*, *Phys. Rev. D* **58** (1998) 094002 [[hep-ph/9806259](https://arxiv.org/abs/hep-ph/9806259)].

[41] K.I. Kudashkin, *to appear*, [XXXX.XXXXX](https://arxiv.org/abs/XXXX.XXXXX).

[42] S. Moch and J.A.M. Vermaseren, *Deep inelastic structure functions at two loops*, *Nucl. Phys. B* **573** (2000) 853 [[hep-ph/9912355](https://arxiv.org/abs/hep-ph/9912355)].

[43] A. Pak, *The toolbox of modern multi-loop calculations: novel analytic and semi-analytic techniques*, *J. Phys. Conf. Ser.* **368** (2012) 012049 [[1111.0868](https://arxiv.org/abs/1111.0868)].

[44] J. Grigo and J. Hoff, *Mass-corrections to double-Higgs production & TopoID*, *PoS LL2014* (2014) 030 [[1407.1617](https://arxiv.org/abs/1407.1617)].

[45] J.S. Hoff, *Methods for multiloop calculations and Higgs boson production at the LHC*, Ph.D. thesis, KIT, Karlsruhe, 2015. 10.5445/IR/1000047447.

[46] P. Nogueira, *Automatic Feynman Graph Generation*, *J. Comput. Phys.* **105** (1993) 279.

[47] J. Hoff, “TopoID: A Mathematica package for the identification of cuts in Feynman diagrams.” <https://github.com/thejensemann/TopoID/>, 2017.

[48] R. Mertig, M. Böhm and A. Denner, *Feyncalc: Computer algebraic calculation of feynman amplitudes*, *Comput. Phys. Commun.* **64** (1990) 345.

[49] V. Shtabovenko, R. Mertig and F. Orellana, *FeynCalc 10: Do multiloop integrals dream of computer codes?*, *Comput. Phys. Commun.* **306** (2025) 109357 [[2312.14089](https://arxiv.org/abs/2312.14089)].

[50] J.A.M. Vermaseren, *New features of form*, *Mathematics and Computers in Simulation* **55** (2001) 1011.

[51] T. van Ritbergen, A.N. Schellekens and J.A.M. Vermaseren, *Group theory factors for Feynman diagrams*, *Int. J. Mod. Phys. A* **14** (1999) 41 [[hep-ph/9802376](#)].

[52] A. von Manteuffel and C. Studerus, *Reduze 2 - Distributed Feynman Integral Reduction*, [1201.4330](#).

[53] J. Grigo, J. Hoff, K. Melnikov and M. Steinhauser, *On the Higgs boson pair production at the LHC*, *Nucl. Phys. B* **875** (2013) 1 [[1305.7340](#)].

[54] M. Höschele, J. Hoff, A. Pak, M. Steinhauser and T. Ueda, *Higgs boson production at the LHC: NNLO partonic cross sections through order ϵ and convolutions with splitting functions to N^3LO* , *Phys. Lett. B* **721** (2013) 244 [[1211.6559](#)].

[55] M. Höschele, J. Hoff, A. Pak, M. Steinhauser and T. Ueda, *MT: A Mathematica package to compute convolutions*, *Comput. Phys. Commun.* **185** (2014) 528 [[1307.6925](#)].

[56] A.V. Kotikov, *Differential equation method: The Calculation of N point Feynman diagrams*, *Phys. Lett. B* **267** (1991) 123.

[57] Z. Bern, L.J. Dixon and D.A. Kosower, *Dimensionally regulated pentagon integrals*, *Nucl. Phys. B* **412** (1994) 751 [[hep-ph/9306240](#)].

[58] M.J.G. Veltman, *Diagrammatica: The Path to Feynman rules*, vol. 4, Cambridge University Press (5, 2012).

[59] J.M. Henn, *Multiloop integrals in dimensional regularization made simple*, *Phys. Rev. Lett.* **110** (2013) 251601 [[1304.1806](#)].

[60] R.N. Lee, *Libra: A package for transformation of differential systems for multiloop integrals*, *Comput. Phys. Commun.* **267** (2021) 108058 [[2012.00279](#)].

[61] R.N. Lee, *Reducing differential equations for multiloop master integrals*, *JHEP* **04** (2015) 108 [[1411.0911](#)].

[62] S. Catani, *The Singular behavior of QCD amplitudes at two loop order*, *Phys. Lett. B* **427** (1998) 161 [[hep-ph/9802439](#)].

[63] R.N. Lee, A.A. Lyubyakin and V.A. Stotsky, *Total cross sections of $e\gamma \rightarrow eX\bar{X}$ processes with $X = \mu, \gamma, e$ via multiloop methods*, *JHEP* **01** (2021) 144 [[2010.15430](#)].

[64] M.A. Barkatou, T. Cluzeau and C. El Bacha, *Frobenius method for computing power series solutions of linear higher-order differential systems*, in *Proceedings of Mathematical Theory of Networks and Systems (MTNS) 2010, Budapest (Hungary)*, p. Inconnu, 2010.

[65] R.N. Lee, A.V. Smirnov and V.A. Smirnov, *Solving differential equations for Feynman integrals by expansions near singular points*, *JHEP* **03** (2018) 008 [[1709.07525](#)].

[66] K.-T. Chen, *Iterated path integrals*, *Bulletin of the American Mathematical Society* **83** (1977) 831.

[67] R.N. Lee, M.D. Schwartz and X. Zhang, *Compton Scattering Total Cross Section at Next-to-Leading Order*, *Phys. Rev. Lett.* **126** (2021) 211801 [[2102.06718](#)].

[68] A.B. Goncharov, *Multiple polylogarithms and mixed Tate motives*, *arXiv preprint math/0103059* (2001) .

[69] H.R.P. Ferguson, D.H. Bailey and S. Arno, *Analysis of pslq, an integer relation finding algorithm*, *Math. Comput.* **68** (1999) 351–369.

[70] X. Liu and Y.-Q. Ma, *AMFlow: A Mathematica package for Feynman integrals computation via auxiliary mass flow*, *Comput. Phys. Commun.* **283** (2023) 108565 [[2201.11669](#)].

[71] C. Duhr and F. Dulat, *PolyLogTools — polylogs for the masses*, *JHEP* **08** (2019) 135 [[1904.07279](#)].

[72] C.W. Bauer, A. Frink and R.B. Kreckel, *Introduction to the GiNaC Framework for Symbolic Computation within the C++ Programming Language*, *J. Symb. Comput.* **33** (2002) 1 [[cs/0004015](#)].

[73] J.C. Collins, F. Wilczek and A. Zee, *Low-Energy Manifestations of Heavy Particles: Application to the Neutral Current*, *Phys. Rev. D* **18** (1978) 242.

[74] S. Qian, *A new renormalization prescription (cwz subtraction scheme) for qcd and its application to dis*, .

[75] I. Bojak, *NLO QCD corrections to the polarized photoproduction and hadroproduction of heavy quarks*, other thesis, 5, 2000, [[hep-ph/0005120](#)].

[76] K. Melnikov and T. van Ritbergen, *The three-loop on-shell renormalization of qcd and qed*, *Nuclear Physics B* **591** (2000) 515 [[hep-ph/0005131](#)].

[77] G.F. Sterman, *An Introduction to quantum field theory*, Cambridge University Press (8, 1993).

[78] G. Altarelli, R.K. Ellis and G. Martinelli, *Large Perturbative Corrections to the Drell-Yan Process in QCD*, *Nucl. Phys. B* **157** (1979) 461.

[79] P.J. Rijken and W.L. van Neerven, *Heavy flavor contributions to the Drell-Yan cross-section*, *Physical Review D: Particles and Fields* **52** (1995) 149 [[hep-ph/9501373](#)].

[80] M. Buza and W.L. van Neerven, $\mathcal{O}(\alpha_s^2)$ contributions to charm production in charged current deep inelastic lepton - hadron scattering, [hep-ph/9702242](#).

[81] T. Gottschalk, *Chromodynamic Corrections to Neutrino Production of Heavy Quarks*, *Phys. Rev. D* **23** (1981) 56.

[82] S. Catani, S. Dittmaier and Z. Trocsanyi, *One loop singular behavior of QCD and SUSY QCD amplitudes with massive partons*, *Phys. Lett. B* **500** (2001) 149 [[hep-ph/0011222](#)].

[83] W.A. Bardeen, A.J. Buras, D.W. Duke and T. Muta, *Deep Inelastic Scattering Beyond the Leading Order in Asymptotically Free Gauge Theories*, *Phys. Rev. D* **18** (1978) 3998.

[84] T. Appelquist and J. Carazzone, *Infrared Singularities and Massive Fields*, *Phys. Rev. D* **11** (1975) 2856.

[85] K.G. Chetyrkin, B.A. Kniehl and M. Steinhauser, *Decoupling relations to $\mathcal{O}\alpha_s^3$ and their connection to low-energy theorems*, [hep-ph/9708255](#).

[86] A. Mitov and S. Moch, *The Singular behavior of massive QCD amplitudes*, *JHEP* **05** (2007) 001 [[hep-ph/0612149](#)].

[87] G. Wang, T. Xia, L.L. Yang and X. Ye, *On the high-energy behavior of massive QCD amplitudes*, *JHEP* **05** (2024) 082 [[2312.12242](#)].

[88] K. Melnikov and A. Mitov, *Perturbative heavy quark fragmentation function through $\mathcal{O}(\alpha_s^2)$* , [hep-ph/0404143](#).

- [89] A.G. Grozin, *Lectures on multiloop calculations*, [hep-ph/0508242](#).
- [90] G. 't Hooft and M.J.G. Veltman, *Regularization and Renormalization of Gauge Fields*, *Nucl. Phys. B* **44** (1972) 189.
- [91] D. Kreimer, *The γ_5 problem and anomalies — a clifford algebra approach*, *Physics Letters B* **237** (1990) 59.
- [92] P. Breitenlohner and D. Maison, *Dimensionally Renormalized Green's Functions for Theories with Massless Particles. 1.*, *Commun. Math. Phys.* **52** (1977) 39.
- [93] P. Breitenlohner and D. Maison, *Dimensionally Renormalized Green's Functions for Theories with Massless Particles. 2.*, *Commun. Math. Phys.* **52** (1977) 55.
- [94] P. Breitenlohner and D. Maison, *Dimensional Renormalization and the Action Principle*, *Commun. Math. Phys.* **52** (1977) 11.
- [95] J.G. Korner, D. Kreimer and K. Schilcher, *A Practicable gamma(5) scheme in dimensional regularization*, *Z. Phys. C* **54** (1992) 503.
- [96] S. Larin and J. Vermaseren, *The alpha-s**3 corrections to the Bjorken sum rule for polarized electroproduction and to the Gross-Llewellyn Smith sum rule*, *Phys. Lett. B* **259** (1991) 345.
- [97] S.A. Larin, *The renormalization of the axial anomaly in dimensional regularization*, *Physics Letters B* **303** (1993) 113.
- [98] S. Larin, *The Renormalization of the axial anomaly in dimensional regularization*, *Phys. Lett. B* **303** (1993) 113 [[hep-ph/9302240](#)].
- [99] G. Passarino and M.J.G. Veltman, *One Loop Corrections for e+ e- Annihilation Into mu+ mu- in the Weinberg Model*, *Nucl. Phys. B* **160** (1979) 151.
- [100] Z. Bern, A. De Freitas and L.J. Dixon, *Two loop helicity amplitudes for gluon-gluon scattering in QCD and supersymmetric Yang-Mills theory*, *JHEP* **03** (2002) 018 [[hep-ph/0201161](#)].
- [101] M. Heller, A. von Manteuffel, R.M. Schabinger and H. Spiesberger, *Mixed EW-QCD two-loop amplitudes for $q\bar{q} \rightarrow \ell^+\ell^-$ and γ_5 scheme independence of multi-loop corrections*, *JHEP* **05** (2021) 213 [[2012.05918](#)].
- [102] S. Moch, J.A.M. Vermaseren and A. Vogt, *On γ_5 in higher-order qcd calculations and the nnlo evolution of the polarized valence distribution*, *Physics Letters B* **748** (2015) 432.